

Articles

3D QSAR Analyses-Guided Rational Design of Novel Ligands for the $(\alpha 4)_2(\beta 2)_3$ Nicotinic Acetylcholine Receptor

Holger Gohlke,^{*,†,§} Simone Schwarz,[†] Daniela Gündisch,[‡] Maria Cristina Tilotta,[‡] Alexander Weber,[†] Thomas Wegge,[†] and Gunther Seitz[†]

Institut für Pharmazeutische Chemie der Philipps-Universität Marburg, Marbacher Weg 6, D-35032 Marburg, Germany, and Institut für Pharmazeutische Chemie der Rheinischen Friedrich-Wilhelms-Universität Bonn, Kreuzbergweg 26, D-53115 Bonn, Germany

Received February 25, 2002

Three-dimensional quantitative structure–activity relationship methods, the comparative molecular field analysis (CoMFA) and the comparative molecular similarity indices analysis (CoMSIA), were applied using a training set of 45 ligands of the $(\alpha 4)_2(\beta 2)_3$ nicotinic acetylcholine receptor (nAChR). All compounds are related to (–)-epibatidine, (–)-cytisine, (+)-anatoxin-a, and (–)-ferruginine, and additionally, novel diazabicyclo[4.2.1]nonane- and quinuclidin-2-ene-based structures were included. Their biological data have been determined by utilizing the same experimental protocol. Statistically reliable models of good predictive power (CoMFA $r^2 = 0.928$, $q^2 = 0.692$, no. of components = 3; CoMSIA $r^2 = 0.899$, $q^2 = 0.701$, no. of components = 3) were achieved. The results obtained were graphically interpreted in terms of field contribution maps. Hence, physicochemical determinants of binding, such as steric and electrostatic and, for the first time, hydrophobic, hydrogen bond donor, and hydrogen bond acceptor properties, were mapped back onto the molecular structures of a set of nAChR modulators. In particular, changes in the binding affinity of the modulators as a result of modifications in the aromatic ring systems could be rationalized by the steric, electrostatic, hydrophobic, and hydrogen bond acceptor properties. These results were used to guide the rational design of new nAChR ligands such as **48–52** and **54**, which were subsequently synthesized for the first time and tested. Key steps of our synthetic approaches were successfully applied Stille and Suzuki cross-coupling reactions. Predictive r^2 values of 0.614 and 0.660 for CoMFA and CoMSIA, respectively, obtained for 22 in part previously unknown ligands for the $(\alpha 4)_2(\beta 2)_3$ subtype, demonstrate the high quality of the 3D QSAR models.

Introduction

Over recent years, there has been steadily increasing interest in nAChR agonists as potential analgesics and therapeutics for the treatment of various neurological and mental disorders related to a decrease in cholinergic function.^{1–4} Thus, for the advancement of nAChR-based therapeutics, many efforts have been directed toward the identification and characterization of novel, potent nAChR ligands. This was stimulated by considerable evidence suggesting that selective neuronal nAChR agonists may provide therapeutic utility in the treatment of Alzheimer's and Parkinson's diseases, attention deficit/hyperactivity disorder, schizophrenia, and depression.^{1,2} Additionally, the discovery of the alkaloidal toxin epibatidine⁵ as a potent analgesic acting via neuronal nAChR has evoked renewed interest in targeting nAChRs also for analgesia.^{6,7} However, the potential therapeutic actions of the prototypical nAChR agonists

such as the natural alkaloids (–)-epibatidine, (–)-nicotine, (–)-cytisine, and (+)-anatoxin-a (Chart 1) are accompanied by a variety of untoward effects.¹ Nevertheless, the emerging diversity of nAChR subtypes opens up the possibility of developing receptor subtype selective therapeutic agents without or with substantially attenuated side effects.

Thus, based upon the approach that bioisosteric alteration in the structures of the various alkaloids might provide nAChR ligands with better ratios of pharmacological to toxicological activity, numerous novel neuronal nAChR ligands have been developed recently.^{8–13} Compounds belonging to class C in Schmitt's classification scheme³ especially constitute the most populated class of nAChR ligands investigated, with both the cationic center and the hydrogen bond acceptor– π moiety (HBA– π) within separate, nonfused rings. In this context, among others, epiboxidine (Chart 1) in which the 5-(2-chloropyridyl) ring of epibatidine has been replaced by the methylisoxazol moiety is worth mentioning.¹⁴ This epibatidine variant proved to be a potent antinociceptive agent with a better activity/toxicity ratio compared to the lead alkaloid. Additionally, UB-165, a hybrid of anatoxin-a and epibatidine in

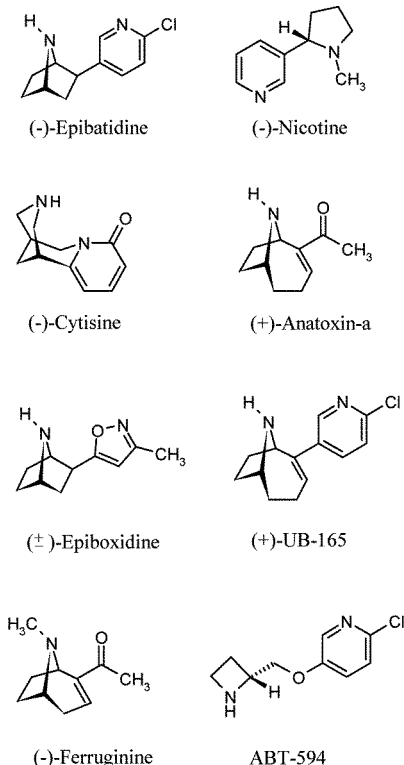
* To whom correspondence should be addressed. Phone: +1-858-784-9788. Fax +1-858-784-8896. E-mail: gohlke@scripps.edu.

[†] Philipps-Universität Marburg.

[‡] Rheinische Friedrich-Wilhelms-Universität Bonn.

[§] Present address: Department of Molecular Biology, The Scripps Research Institute, La Jolla, CA 92037.

Chart 1. Alkaloid nAChR Ligands Such as (–)-Epibatidine, (–)-Nicotine, (–)-Cytisine, and (+)-Anatoxin-a and the Synthetic nAChR Ligands (±)-Epiboxidine, (+)-UB-165, (–)-Ferruginine, and ABT-594



which the acetyl group of anatoxin-a is replaced by a 5-(2-chloropyridyl) ring, was reported to show significant nAChR binding affinity and stimulant activity.^{8,11}

Under development as a potent broad-spectrum analgesic is ABT-594,⁷ a novel 3-pyridyl ether nAChR agonist that demonstrates a superior selectivity for neuronal nAChRs and, consequently, an improved in vivo side-effect profile compared with epibatidine.

Our recent efforts aim at the development of novel semi-synthetic variants of highly potent nAChR ligands that show a subtype profile toward the central, heteropentameric $(\alpha 4)_2(\beta 2)_3$ nAChR (the main subtype found in brain tissue), eliminating interactions with the ganglionic subtype. Until now, we have successfully pursued this goal by synthesizing compounds following a more traditional approach. By combining the “trial and error” method with bioisosteric or other modifications of the alkaloidal toxins (–)-epibatidine,^{15,16} (–)-cytisine,¹⁷ (+)-anatoxin-a,^{18,19} or (–)-ferruginine,^{19–23} as well as diazabicyclo[4.2.1]nonane- and quinuclidin-2-ene-based variants,^{24,25} we obtained ligands with promising therapeutic utility.

Although pharmacophore models for subtypes of nAChRs had been long known,^{26–30} only recently the high-resolution three-dimensional (3D) structure of a soluble, homopentameric molluscan acetylcholine-binding protein (AChBP) has been determined by protein crystallography.³¹ Even though this structure reveals the essential features and the organization of the key region of the agonist binding site³¹ and shows significant sequence similarity with the extracellular parts of the nAChR subunits, a 3D model of the extracellular domain of $(\alpha 4)_2(\beta 2)_3$, a prerequisite for a structure-based

design, has only been published after our work had been completed.³² Hence, in this study, we decided to perform three-dimensional quantitative structure–activity relationship (3D QSAR) analyses to guide a ligand-based rational design process aiming at the improvement of the binding affinity of our lead compounds toward $(\alpha 4)_2(\beta 2)_3$.

To our knowledge, only a few QSAR studies for agonists of nAChRs have been reported to date,^{30,33} with Nicolotti et al.³⁴ being the most comprehensive one in terms of chemical classes of nicotinic agonists analyzed. Despite deriving a generic model comprising all different classes, the latter study especially notes the importance of analyzing congeneric series separately, resulting in more precious indications on physicochemical interactions. This becomes even more important in light of two recent studies of Dougherty and co-workers^{35,36} that strongly suggest that pharmacophore models for the muscle-type nAChR should be expanded to include distinct agonist binding modes for ACh-like compounds and nicotine-like compounds, respectively. In the case of 3D QSAR analyses, however, it is necessary that all compounds considered adopt a similar binding mode.

In our study, 3D QSAR analyses (i.e., comparative molecular field analysis (CoMFA) and comparative molecular similarity indices analysis (CoMSIA)) were performed on a data set of 45 agonist compounds related to (–)-epibatidine, (–)-cytisine, (+)-anatoxin-a, and (–)-ferruginine; additionally, diazabicyclo[4.2.1]nonane- and quinuclidin-2-ene-based nAChR ligands were included in the training set and in the test set. To the best of our knowledge, this is the most comprehensive data set of “polycyclic derivatives” (following the classification of Nicolotti et al.³⁴) applied in 3D QSAR analyses of ligands of the $(\alpha 4)_2(\beta 2)_3$ nAChR. In addition, all biological data were determined with our recently published radio ligand binding assay.¹⁸ This is expected to improve the signal-to-noise ratio in the biological data compared to collecting affinity data from different laboratories or experimental protocols.³

Both 3D QSAR techniques compare a series of molecules in terms of molecular interaction fields, that is, they correlate field differences with differences in the dependent target property, here the binding affinity. For CoMFA,³⁷ interaction fields are represented as steric and electrostatic interaction energies calculated for a molecule in the data set at the intersections of a grid embedding that molecule. Alternative molecular interaction fields are applied in CoMSIA.³⁸ Gaussian functions are used to describe steric, electrostatic, and hydrophobic similarities. Similarly, hydrogen bond donor and acceptor properties are considered.³⁹ Compared to CoMFA, this approach avoids particularly steep potentials next to molecular surfaces and, thus, allows determining similarity indices close to the atoms, too. Regarding the interpretation of 3D QSAR results in terms of field contribution maps, CoMSIA denotes those areas *within the regions* occupied by the ligands that favor or disfavor the presence of a group of particular physicochemical property. In contrast, CoMFA highlights those areas where the ligand would interact with a possible environment.⁴⁰ Additionally, contribution maps have been reported to be more contiguous for CoMSIA than for CoMFA, facilitating the interpretation

of the results of the former model.⁴⁰ In fact, no electrostatic maps have been given for the CoMFA model of "polycyclic derivatives" in the study of Nicolotti et al.³⁴ because they were "hard to be completely understood". We have shown recently, however, that subtle electrostatic influences of especially the heteroaromatic moiety result in significant differences in binding affinities of (+)-anatoxin-a-related agonists.¹⁸ Hence, exploiting these interaction maps from the CoMSIA model might provide an interesting alternative.

Finally, the field contribution maps of the statistically significant QSAR models were interpreted to generate ideas for new nAChR ligands that might be more active than our lead compounds already included in the training set. After ranking the hypothetical molecules by predicted binding affinities, several candidates (**48–52**, **54**, and **56–63**) were synthesized for the first time and included in our test set. Key steps of our synthetic approaches were Stille and Suzuki cross-coupling reactions. Subsequent biological testing of the new compounds yielded an experimental validation of the satisfying predictive power of our 3D QSAR models. Applying the derived models for the design of new compounds again clearly distinguishes our study from former QSAR studies on nAChR agonists.

Methods

All molecular modeling and comparative molecular field evaluations were performed using SYBYL⁴¹ version 6.6 running on a Silicon Graphics Indigo2 workstation.

Data Set and Alignment. A training set of 45 ligands (Table 1) was used for all CoMFA and CoMSIA analyses. Compounds **12**, **16**, **18**, **19**, and **29–37** thereof are reported in this study for the first time. Since the use of charged or uncharged molecules in comparative modeling is still a matter of debate,⁴² 3D QSAR analyses were performed with molecules either protonated or unprotonated at the nitrogen of the bicycle. Here, only a small influence on the statistical results is expected because of the fact that CoMFA and CoMSIA only relate differences in molecular structure to differences in binding affinities, and the change in protonation state affects all molecules in equal measure. The molecules are structurally close to the natural alkaloids epibatidine (**1**),⁵ ferruginine (**17**),⁴³ anatoxin-a (**20**),⁴⁴ or cytisine (**39**).¹⁷ In the novel ligands **29** and **30**, the bicyclic pharmacophoric element is represented by a quinuclidin-2-ene moiety²⁵ and, in compounds **34–37**, by a novel diazabicyclo[4.2.1]nonane scaffold.²⁴ According to the classification of Schmitt,³ the compounds are characterized by the requisite pharmacophoric elements typical of nAChR ligands. Some of them, for example, **25–28** and the cytisines **38–45**, are class E³ compounds where both the cationic and HBA- π sites are contained within a fused polycyclic ring system. Most of the molecules are class C ligands,³ which show both the N-bicycle and the HBA- π system within separate, nonfused rings. These two pharmacophoric elements are joined by a pivot bond. The rotational barriers at this central bond of the ligands lead to a mixture of minimum conformations in solution at room temperature with different inter-nitrogen distances more or less suitable for a ligand-nAChR interaction.

Unfortunately, until today neither the structure of the vertebrate nAChR receptor nor the structure of a

ligand-receptor complex has been solved at the atomic level.³¹ As a result, the biologically active conformation of the ligands is not known. To test the influence of the alignment on the outcome of the analyses, two different strategies were pursued.

On one hand, a conformational search for some compounds containing a pivot bond between the azabicyclic and the N-heterocycle indicated the existence of only two favorable orientations of both rings with respect to each other.^{11,18} Hence, to obtain a consistent alignment, the dihedral angle τ of the pivot bond (as defined, e.g., for UB-165 and epibatidine³³) between these two pharmacophoric elements was initially set to 30°, a value close to the ones found in the conformational search. The generated conformations were subsequently minimized without restraints with MOPAC 6.0,^{45,46} using the AM1 Hamiltonian.⁴⁷ In the resulting conformations of the (unprotonated) compounds UB-165 and epibatidine, values of $\tau = 54^\circ$ and 31° , respectively, are in good agreement with those determined by Tonder et al.³³ (56° and 20° , respectively). Additionally, the compounds fulfill the criteria for the distance between the bicycle-N and the heterocycle-N as given by the Sheridan model.²⁶ Similar findings also hold for the protonated compounds. The molecules were then rigidly aligned by applying the RigFit method.⁴⁸ RigFit uses a Gaussian function representation describing chemical features of the ligands such as steric occupancy, positive and negative partial charge, hydrophobicity, and hydrogen bonding properties.⁴⁸ Hence, this procedure accounts for the ligands in total and not only for selected pharmacophoric elements. In view of the restricted conformational flexibility of the molecules, a rigid alignment of properly determined conformations seemed appropriate in this case. Although more active and equally rigid ligands were in the training set, **10** was chosen as a reference compound because it (a) shows the highest binding affinity of the ferruginine-related compounds with the HBA- π -pharmacophoric element in the 2-position and (b) represents a compromise in structural terms with respect particularly to the different types of bicyclic systems. In principle, a few alignments were predicted by RigFit for each molecule. The final one was chosen such that the interaction geometries of the pharmacophoric elements of the nAChR modulators, as postulated by Sheridan,²⁶ were aligned best. These pharmacophoric elements are:

(A) a quaternary or protonatable nitrogen (e.g., of the aliphatic bicycle in anatoxin-a (**20**))

(B) an electronegative atom as hydrogen bond acceptor (e.g., the pyridine nitrogen of epibatidine (**1**) or a carbonyl oxygen of the acetyl group in anatoxin-a (**20**))

(C) an atom that forms a dipole with B (the carbonyl carbon, e.g., in anatoxin-a (**20**) or a so-called dummy point in the case of the center of the pyridine ring, e.g. in epibatidine (**1**)); the line connecting B and C defines the direction of the local dipole moment along which a hydrogen bond is likely to be formed.

Alternatively, a flexible alignment applying the program TorSeal⁴⁹ was performed, again using the above-determined conformation of **10** as a rigid reference. TorSeal first generates an alignment of multiple rigid conformations by a global search operation and then conformationally relaxes the best-scored hits of this

Table 1. Data Set of 45 Compounds Used in the Training Set and 22 Compounds Used To Predict Binding Affinities^a

No.	Structure	R	K _i	Ref.	pK _i	ΔpK _i		No.	Structure	R	K _i	Ref.	pK _i	ΔpK _i	
						CoMFA	CoMSIA							CoMFA	CoMSIA
Training Set															
1 ^b			0.008 ± 0.0002	20	11.10	0.210	0.459	31			1659 ± 354	22	5.78	0.052	-0.902
2 ^b			0.029 ^c	13	10.55	-0.170	0.194	32			9.6	22	8.02	0.496	0.060
3 ^b			0.045 ± 0.0025	13	10.35	-0.382	-0.546	33			43.2	22	7.36	-0.329	-0.539
4 ^b			0.025 ^c	13	10.60	-0.418	-0.514	34			0.873	24	9.06	-0.706	-0.071
5 ^b			0.027 ± 0.0016	13	10.57	-0.015	0.876	35			0.55 ± 0.15	24	9.26	-0.302	0.368
6 ^b			0.028 ± 0.0026	13	10.55	-0.045	1.203	36			265	24	6.58	0.213	0.597
7 ^b			0.036 ± 0.0042	13	10.44	-0.292	0.321	37			2.08 ± 0.14	24	8.68	0.615	1.061
8		-COCH ₃	94 ± 2.1	16,20	7.03	-0.368	-0.307	38		-	5.7 ± 1.5	17	8.24	-0.792	0.457
9			400 ± 17	20	6.40	-0.043	-0.186	39		R ¹ = H R ² = H	0.123 ± 0.01	17	9.91	0.453	0.092
10			3.7 ± 0.6	20	8.43	0.369	-0.175	40		R ¹ = Cl R ² = Cl	2.5 ± 0.4	17	8.60	-0.049	-0.922
11			8 ± 1.1	16,20	8.10	0.276	-0.005	41		R ¹ = Br R ² = Br	10.8 ± 0.4	17	7.97	-0.253	-0.603
12			4 100 ± 300	19	5.38	-0.214	-0.479	42		R ¹ = Br R ² = H	0.010 ± 0.001	17	11.00	0.973	0.651
13 ^b			31 ± 2.4	19	7.51	0.353	0.405	43		R ¹ = H R ² = Br	0.308 ± 0.014	17	9.51	0.803	-0.199
14 ^b			0.66 ± 0.04	19	9.18	0.516	0.048	44		R ¹ = H R ² = I	0.230 ± 0.02	17	9.64	0.777	-0.420
15 ^b			10 ± 2.3	16	8.00	-0.162	-0.564	45			0.832 ± 0.056	17	9.08	0.459	0.532
16 ^b			210 ± 25	19	6.68	0.082	0.078	Test Set							
17		-COCH ₃	120 ± 7.5	16,20	6.92	0.304	0.509	46 ^b			0.026	10	10.59	-0.186	0.997
18		-CON(CH ₃) ₂	2 000 ± 156	19	5.70	0.006	-0.065	47			30 ± 1.2	16	7.5	0.771	0.727
19		-CSN(CH ₃) ₂	>2x10 ⁴	19	<4.70	-0.249	-0.348	48		-CON(CH ₃) ₂	6.1x10 ⁴ ± 4300	19	4.21	-1.817	-2.129
20		-COCH ₃	1.1 ± 0.2	18	8.96	0.198	0.581	49		-CSN(CH ₃) ₂	2x10 ⁴ ± 3400	19	5.61	-0.425	-0.090
21			0.17 ^c	8, 18	9.77	0.489	-0.396	50			2 ± 0.5	19	8.70	-0.054	-0.687
22			12 ± 1.8	18	7.92	0.020	0.465	51			1.6 ± 0.2	19	8.80	1.314	0.262
23			0.14 ± 0.03	18	9.85	0.361	0.476	52 ^b			0.708 ± 0.04	19	9.15	0.096	-0.376
24			19 ± 2.5	18	7.72	-1.093	-0.994								
25			>10 ⁴	21	<5.00	-0.591	0.230								
26 ^b			676 ± 26	21	6.17	-0.144	-0.361								
27			76 ± 4.4	21	7.12	-0.105	-0.751								
28			35 ± 3.2	21	7.46	-0.062	0.453								
29			12.2 ± 0.18	25	7.91	-0.897	-0.296								
30			2.28 ± 0.05	25	8.64	-0.345	-0.472								

Table 1 (Continued)^a

No.	Structure	R	K _i	Ref.	pK _i	ΔpK _i		No.	Structure	R	K _i	Ref.	pK _i	ΔpK _i	
						CoMFA	CoMSIA							CoMFA	CoMSIA
Test Set															
53 ^b			0.257 ± 0.06	19	9.59	1.483	0.499	61			12.6 ± 0.07	23	7.90	0.418	0.140
54			0.151 ± 0.02	19	9.82	0.012	-0.233	62			8.9	22	8.05	0.296	-0.753
55			0.051 ± 0.006	18	10.29	1.650	1.083	63			0.528 ± 0.11	24	9.28	1.282	2.035
56			7.6 ± 0.49	25	8.12	-0.189	0.030	64			0.520 ± 0.015	17	9.28	0.490	-1.440
57 ^b			1.54 ± 0.02	22	8.81	0.131	-0.151	65			0.022 ± 0.005	17	10.65	1.127	0.486
58 ^b			1.25	22	8.90	0.413	0.974	66			0.017 ± 0.002	17	10.77	1.164	0.204
59			4931 ± 144	22	5.31	0.166	-0.422	67			2.5 ± 0.3	17	8.60	-0.630	-1.034
60			212	22	6.67	1.106	0.969	<i>r</i> ² _{pred} ^{d)}					0.614	0.660	

^a The experimental binding affinities toward the (α4)₂(β2)₃ nAChR subtype are expressed as pK_i (-log K_i) values. K_i is given in nM. ΔpK_i is the error of fitted (training set) or predicted (test set) binding affinities and is given as (pK_{i,actual} - pK_{i,fitted/predicted}). ^b Racemate. ^c Average of published data. ^d Predicted *r*² calculated with a standard deviation (SD) obtained from the test set: 0.617 (CoMFA), 0.657 (CoMSIA).

global search. The description of the molecules by shape-associated physicochemical properties in space extends the SEAL procedure⁵⁰ and resembles RigFit. Again, the final alignment of each molecule was chosen among the first TorSeal solutions such that the geometric criteria given by the Sheridan model were fulfilled. Ligand coordinates of all molecules used in the analyses can be obtained from us upon request.

The experimentally determined biological affinities of the nAChR ligands are given as pK_i values (Table 1). The affinities of the 45 training set compounds spread over a satisfactorily large range of pK_i values from 4.7 to 11.10, that is, 6.4 orders of magnitude.^{51,52} A similar range and distribution of pK_i was obtained for the 22 test set compounds.

CoMFA and CoMSIA Analysis. Steric and electrostatic CoMFA fields were calculated as implemented in SYBYL⁴¹ using Lennard-Jones and Coulombic potentials, respectively.³⁷ Partial atomic charges were determined using the AM1 Hamiltonian⁴⁷ within the semiempirical package MOPAC.^{45,46}

All calculations were performed with SYBYL standard parameters using an sp³-hybridized carbon probe atom with a charge of +1.0 for the calculation of steric and electrostatic CoMFA fields. The five physicochemical properties for CoMSIA (steric, electrostatic, hydrophobic, and hydrogen bond donor and acceptor) were evaluated using a common probe atom with 1 Å radius, +1.0 charge, and hydrophobicity and hydrogen bond property values of +1. The value of the so-called attenuation factor α was 0.3.

To test the influence of the grid spacing on the statistical results, lattices of 1 and 2 Å spacing, respectively, were applied for the calculation of interaction fields. The box sizes were chosen such that all molecules were sufficiently embedded with a margin of at least 4 Å. To allow a comparison of CoMFA and CoMSIA

Table 2. Parameters of the Grid Boxes Used for CoMFA and CoMSIA Analyses

	<i>x</i>	<i>y</i>	<i>z</i>	<i>x</i>	<i>y</i>	<i>z</i>
grid spacing		1 Å			2 Å	
lower corner	-9.0	-5.0	-9.0	-9.0	-5.0	-9.0
higher corner	8.0	10.0	8.0	8.0	10.0	8.0
number of steps	18	16	18	9	8	9
points	5184			648		

results, equal box coordinates were used in both cases. The parameters of the grid boxes are given in Table 2. CoMFA and CoMSIA fields were subsequently calculated as described above. PLS^{53,54} analyses were performed following the standard implementation in SYBYL.

To check the statistical significance of the models, cross-validations were done by means of the "leave-one-out" (LOO) procedure using the enhanced version of PLS, the SAMPLS⁵⁵ method. The optimal number of components was determined in such a way that each additional component had to increase the *q*² (cross-validated *r*²) by at least 5%. This approach considers the "parsimony-principle"⁵² by selecting the smallest number of significant components. In our case, this procedure yielded models with fewer components compared to the use of the minimal *s*_{PRESS} value to determine the optimal number of components. The same number of components was subsequently applied to derive the final QSAR models. Here, in the case of CoMFA, the "minimum σ" standard deviation ("column filtering" in SYBYL) was set to a threshold of 1 kcal/mol, resulting in approximately 10% of the columns considered in the PLS analysis. For CoMSIA, where field values are given in arbitrary units and, hence, no physical unit can be defined for the threshold value, a σ-value was chosen such that a similar amount of columns is taken into account. Variations of these values did not significantly influence the outcome of the calculations, however. The statistical results are sum-

Table 3. Summary of Results from the CoMFA and CoMSIA Analyses

	CoMFA	CoMSIA	CoMFA	CoMSIA	CoMFA	CoMSIA	CoMFA	CoMSIA
alignment		rigid		rigid		rigid		flexible
grid spacing		1 Å		2 Å		1 Å		1 Å
bicycle-N		unprotonated		unprotonated		protonated		unprotonated
q^2	0.692	0.701	0.623	0.709	0.503	0.590	0.528	0.601
SPRESS	0.973	0.958	1.090	0.945	1.235	1.122	1.204	1.134
r^2	0.928	0.899	0.937	0.904	0.873	0.834	0.888	0.896
S	0.470	0.556	0.445	0.544	0.624	0.715	0.586	0.579
F	176.638	122.174	148.968	128.312	94.213	68.446	108.533	67.224
components	3	3	4	3	3	3	3	5
fraction								
steric	0.401	0.033	0.476	0.032	0.541	0.035	0.452	0.048
electrostatic	0.599	0.140	0.524	0.151	0.459	0.110	0.548	0.139
hydrophobic		0.259		0.252		0.295		0.280
donor		0.266		0.261		0.221		0.270
acceptor		0.302		0.304		0.340		0.263

marized in Table 3. The q^2 , s_{PRESS} , r^2 , and S values were computed as defined in SYBYL. The most significant 3D QSAR analyses were obtained for the unprotonated compounds, which were aligned with RigFit. While the predictive power of CoMSIA analyses obtained for grid spacings of 1 or 2 Å is comparable, a more significant CoMFA model is obtained with a 1 Å grid (see also Results and Discussion). Hence, unless otherwise stated, results are reported for rigidly aligned, unprotonated compounds using a 1 Å grid spacing.

The plots of predicted versus actual binding affinities for the fitted PLS analyses are shown in Figure 1.

Additionally, to perform an even more rigorous statistical test, several runs of a "leave-five-out" procedure were performed, providing q^2 values similar to those from the corresponding LOO results (see Supporting Information).

A common test to check the consistency of the models is to scramble the biological data and repeat the model derivation process, thus allowing detection of possible chance correlations. After randomizing our data set, solely values of $q^2 < 0$ were observed in the PLS analyses.

As shown in Table 1, compounds **1–7**, **13–16**, and **26** (training set) and **46**, **52**, **53**, **57**, and **58** (test set) were used as racemates for biological testing. The biological affinity of nAChR ligands is in most cases enantioselective.^{8,30,56} To consider the case that the other enantiomer might be completely inactive, the K_i values of these compounds were doubled and model derivation repeated. However, since only minor changes in the statistical parameters were observed (see Supporting Information), the original pK_i values were used in the final model.

To graphically interpret the 3D QSAR results in terms of field contributions, isocontour maps were generated using the field type "stdev*coeff". To select appropriate contour levels for each feature, the resulting histograms of actual field values were analyzed. In an iterative manner, a contour level was chosen that produces the best interpretable contour map.⁵⁷ These contour maps were then used to guide the design of new potential $(\alpha_4)_2(\beta_2)_3$ nAChR ligands.

After ranking by the predicted binding affinities, several candidates (the most promising as well as two with an affinity predicted to be in the μM range) were synthesized and tested. Finally, the calculated and the experimentally determined binding affinities of the

newly designed (**48–52** and **54**) and 16 partly known nAChR ligands (**46**, **47**, **53**, and **55–67**) were compared, again providing a test to assess the predictive power of the computed CoMFA and CoMSIA models (Table 1). The predictive r^2 was calculated according to the definition of Cramer et al.³⁷ The plots of predicted versus actual binding affinity for the test set molecules are shown in Figure 2.

In Vitro Receptor Binding. In this study, a previously developed competition assay for the $(\alpha_4)_2(\beta_2)_3$ nAChR subtype with (\pm) -[³H]epibatidine and P2 membrane fractions of Sprague–Dawley rat forebrains was utilized. The specific binding of (\pm) -[³H]epibatidine to crude synaptic membranes of rat forebrain, at concentrations up to 800 pM, is characterized by a single population of binding sites with $K_d = 8 \pm 0.3$ pM.^{18,58} Similar high-affinity binding of (\pm) -[³H]epibatidine was observed in the rat,⁵⁹ mouse,⁶⁰ human brain,⁶¹ and in transfected cells stably expressing the $(\alpha_4)_2(\beta_2)_3$ nAChR subtype.⁶²

Results and Discussion

Chemistry. The synthetic route to various enantiopure ferrugininoids (structurally related to $(-)$ -ferruginine), such as the potential ligands **18**, **19**, **48**, and **49** in which the acetyl moiety of the lead is bioisosterically replaced by a carboxamide or thiocarboxamide group, started with anhydroecgonin⁶³ (**68**) as the chiral building block (Scheme 1). Treatment of **68** with dimethylammonium chloride/thionyl chloride in benzene yielded the dimethylamide **18** in good yield, which could be transformed to the corresponding thioamide **19** with tetraphosphorus decasulfide/sodium fluoride in DME as sulfur transfer reagent.⁶⁴ Demethylation of **18** by treatment with ethyl chloroformate in the presence of potassium carbonate⁶⁵ afforded the carbamate **69**. Subsequent deprotection with trimethylsilyl iodide (TMSI) in boiling chloroform⁶⁶ followed by treatment with sodium methoxide in methanol led to the *N*-8-demethylated dimethylamide **48** that could be easily converted to the corresponding thioamide **49** with 73% yield.

The novel chlorodiazine-containing ferrugininoids **12**, **16**, **50**, and **52**, the pyridyl-substituted analogues **51** and **53**, as well as the anatoxinoid **54** were synthesized as depicted in Scheme 2. A key step for the preparation of the diazines **12**, **16**, **50**, **52**, and **54** was a palladium-catalyzed Stille cross-coupling⁶⁷ of the tributylstannyll chlorodiazines **72** and **74** with the vinyl triflates **71**, **79**,

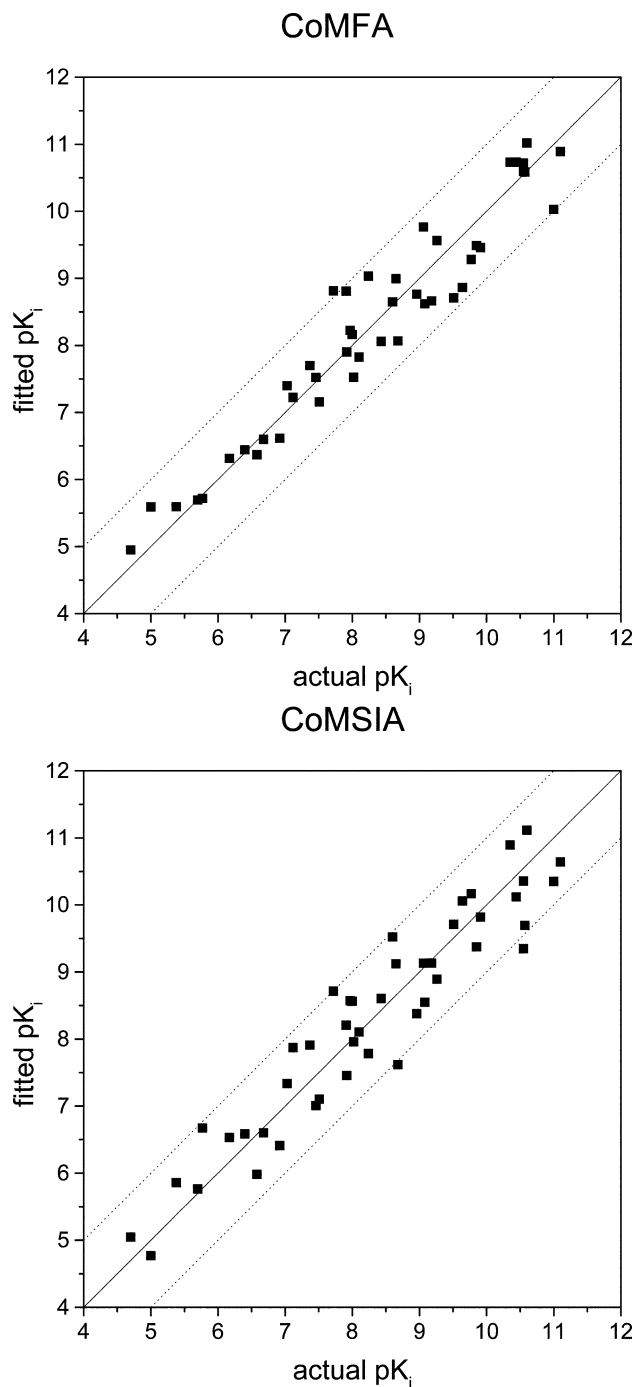


Figure 1. Fitted predictions versus actual binding affinities for the 45 compounds of the training set. The predicted values were obtained by PLS analyses using the CoMFA (top) and CoMSIA (bottom) method. In addition to the line of ideal correlation, dotted lines are given, which indicate deviations from the actual pK_i by ± 1 logarithmic unit.

and **84** of the corresponding carbamate protected ketones, the 2-tropanone **70**, the 3-tropanone **78**, and the 2-homotropone **83**. Optimal overall yields of the desired coupling products **73**, **75**, **80**, **81**, and **85** were reproducibly achieved in the presence of 10 mol % of bis(benzonitrile)palladium(II) chloride as the catalyst under conditions recently described by us for the syntheses of several diazine-containing bioisosteres of (+)-UB 165.¹⁸ The introduction of the 3-pyridyl unit into the bulky tropane moiety could be successfully realized by a Suzuki-type cross-coupling of the vinyl triflates **71**

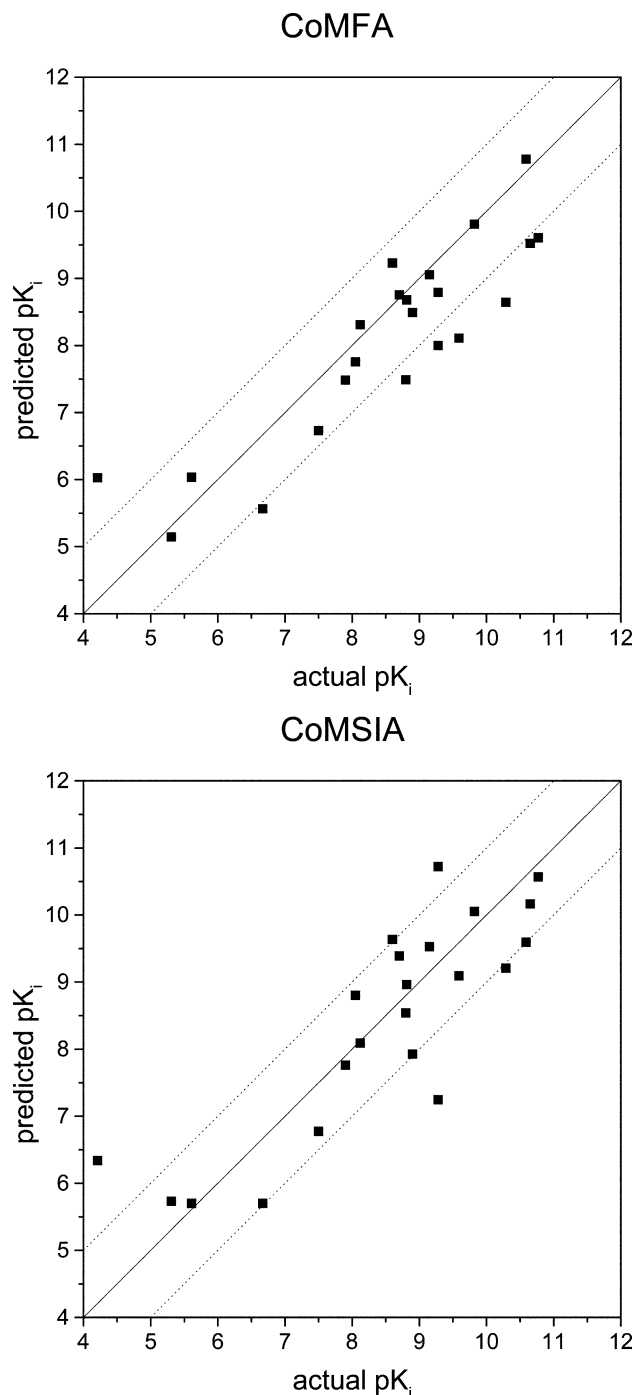
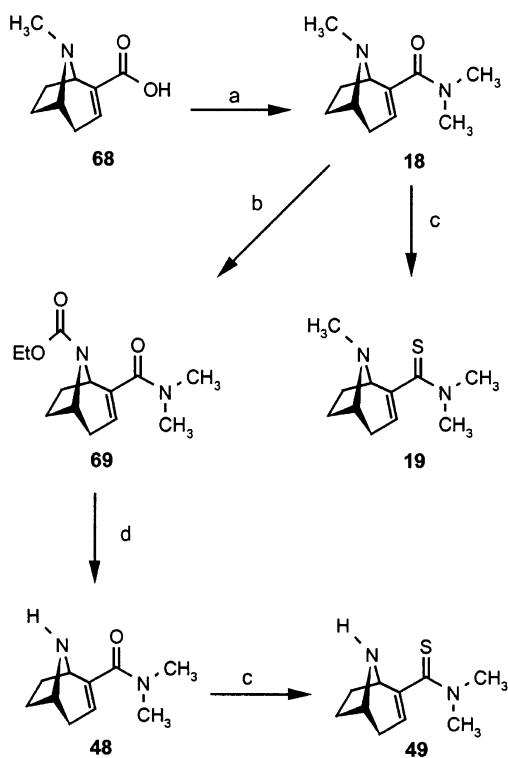


Figure 2. Predicted versus actual binding affinities for the 22 compounds not included in the training set. The predicted values were obtained from the CoMFA (top) and CoMSIA (bottom) models for rigidly aligned, neutral molecules using a 1 Å grid spacing. In addition to the line of ideal correlation, dotted lines are given, which indicate deviations from the actual pK_i value by ± 1 logarithmic unit.

and **79** with the 3-diethylboranylpyridine (**76**).⁶⁸ Bis-(triphenylphosphane)palladium(II) chloride was used as a catalyst and aqueous sodium carbonate as a nucleophilic activator, affording the carbamate-protected target compounds **77** and **82**. Removal of the protecting group in the last step utilizing the synthetic protocol with TMSI in boiling chloroform afforded the novel potential nAChR ligands **12**, **16**, and **50–54** with satisfying yields (see Experimental Section). The nAChR ligands **12**, **16**, **18**, **19**, and **48–54** exhibited the expected

Scheme 1^a

^a Reagents and conditions: (a) $(\text{H}_3\text{C})_2\text{NH}_2\text{Cl}$, C_6H_6 , then SOCl_2 , reflux, 3 h; (b) ClCO_2Et , K_2CO_3 , C_6H_6 , reflux, 12 h; (c) P_4S_{10} , NaF , DME , rt, 20 h; (d) $(\text{CH}_3)_3\text{SiH}$, CHCl_3 , 80°C , 3.5 h, then $\text{NaOCH}_3/\text{CH}_3\text{OH}$.

^1H and ^{13}C NMR, IR, and mass spectral characteristics and gave satisfactory high-resolution mass spectral data. The syntheses and the preliminary biological profile of the compounds **29–37**, **56**, and **58–63** will be published elsewhere soon.

Predictive Power of 3D QSAR Analyses. With a properly selected data set of 45 modulators of the $(\alpha 4)_2(\beta 2)_3$ nAChR (class C and E compounds in Schmitt's³ classification), all QSAR models derived are statistically significant and show a high degree of predictive power (Table 3). The $\text{p}K_i$ values of the compounds, all determined utilizing the same experimental protocol in our laboratory, cover a range of more than 6 orders of magnitude and are uniformly distributed. With respect to the size of the training set, Nicolotti et al.³⁴ recently noted the importance of an in-depth analysis of a congeneric series of molecules, which yielded better information on specific physicochemical interactions compared to a comprehensive QSAR model. Hence, having in mind the design of improved ligands that are accessible via the synthetic route recently developed by us, we did not intend to grossly exceed the chemical subspace represented by our training set compounds. In our opinion, having a more restricted set of training compounds, yet with highly accurate biological data, should be preferred over a set of structurally more diverse compounds related to lower-quality biological data.

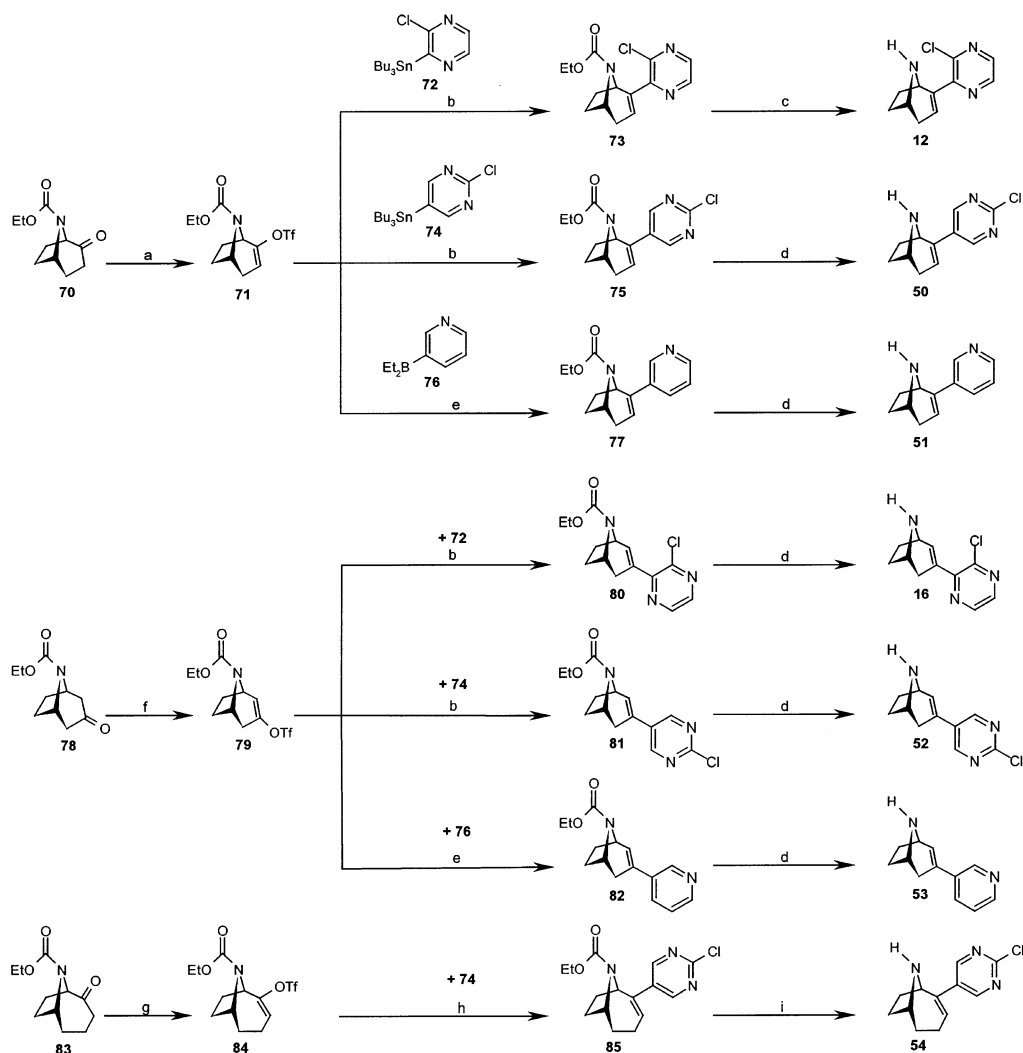
The CoMSIA analyses of the unprotonated, rigidly aligned compounds revealed the models of highest qualities ($q^2 = 0.701$ (0.709) for 1 \AA (2 \AA) grid spacing) (Table 3). The model derived by CoMFA analysis for the same data set shows only a slightly smaller q^2 value in

the case of a 1 \AA grid ($q^2 = 0.692$). A loss in quality is observed in the case of CoMFA where a lattice of 2 \AA spacing has been used for calculating the interaction fields ($q^2 = 0.623$). Obviously, these fields contain less information. Hence, unless otherwise stated, results are reported for rigidly aligned, unprotonated compounds using a 1 \AA grid spacing.

The plots in Figure 1 do not reveal any systematic over- or under-prediction for parts of the activity range. Furthermore, no trend can be observed for residuals across different classes of compounds. Thus, both observations suggest that the present 3D QSAR models represent the whole data set of compounds.

Because both the CoMFA and CoMSIA models show comparable statistical significance as expressed by similar q^2 values, the inclusion of three additional fields in CoMSIA compared to those in the CoMFA method does not seem to be justified from a statistical point of view. While using the hydrogen bond donor or hydrophobic field alone does not result in a statistically significant model, CoMSIA analyses with the steric ($q^2 = 0.475$), electrostatic ($q^2 = 0.668$), and hydrogen bond acceptor field ($q^2 = 0.477$) alone resulted in q^2 values close to or beyond 0.5. Similar q^2 values were also found for all combinations, including two to four field types. This finding corroborates the assumption that strong intercorrelations prevail among the fields.⁶⁹ This effect can also be seen by the contribution of the steric field: although the steric effect amounts to 40% in CoMFA, it is only 3% in CoMSIA. On one hand, omitting the steric field from the CoMSIA analysis results in a q^2 value of 0.703, almost identical to the one reported for the complete analysis. On the other hand, calculations omitting, in turn, one of the electrostatic, hydrophobic, or hydrogen bond donor or acceptor fields revealed that none of these fully accounts for the decrease in the steric contribution alone because in all cases, the contribution of the steric effect remained <6.5%. Despite these obvious interdependencies, however, we decided to consider all five different property fields in CoMSIA because they allow the partitioning of the 3D QSAR results with respect to a more detailed description of physicochemical determinants for binding of the molecular structures.

When ionizable compounds are involved, one must decide which protonation state of the molecules to use in the calculations.⁴² CoMFA and CoMSIA analyses obtained for compounds being protonated at the bicyclic-N also resulted in statistically significant models, yet with lower q^2 values (CoMFA: 0.503; CoMSIA: 0.590) compared to the results obtained with neutral species. Changes in the protonation state affect a similar region in all molecules and, thus, do not lead to large changes in the structural differences among the data set. This may explain why the influence of the protonation state of the molecules on the predictive power of the models is still moderate. This is also demonstrated by the similar contribution of the electrostatic field in the case of CoMSIA, although the contribution of the electrostatic field in the case of CoMFA analysis of protonated compounds is reduced compared to that in the analysis of neutral molecules. Comparable results are also found using the flexibly aligned data sets (data not shown).

Scheme 2^a

^a Reagents and conditions: (a) ref 15; (b) Pd(PhCN)₂Cl₂, Ph₃As, CuI, LiCl, DMF, 85 °C, then KF, CH₃OH; (c) aqueous hydrochloric acid (37%), 80 °C, 1 h, then aqueous NH₃ – pH = 9; (d) (CH₃)₃SiI, CHCl₃, 85 °C, 3 h, then HCl in (C₂H₅)₂O, CH₃OH, 10 min, rt; (e) Pd(PPh₃)₂Cl₂, THF, 2 M aqueous Na₂CO₃, 85 °C; (f) ref 16; (g) ref 16, 18; (h) analogous (b), 80 °C, 12 h; (i) analogous (d) but 80 °C, 3 h, then 1 M aqueous hydrochloric acid. Ligands **50**, **52**, and **54** were isolated as the corresponding hydrochloride salts and ligand **53** was isolated as the maleate salt.

Finally, to test the influence of the alignment on the outcome of the 3D QSAR analyses, the neutral molecules were flexibly aligned onto **10**. Hereby, **10** was held rigid to provide a reference that best complies with the geometric criteria given by the Sheridan model. Again, although the resulting QSAR models showed less predictive power (CoMFA: $q^2 = 0.528$; CoMSIA: $q^2 = 0.601$) than the ones obtained with the rigidly aligned molecules, both models are statistically significant. Overall, obtaining comparable results for two independently aligned sets of molecules supports the significance of both.

Graphical Interpretation of the Fields. In the following figures, the isocontour diagrams of the field contributions (“stdev*coeff”) of different properties as found by the CoMFA and CoMSIA analyses are illustrated together with exemplary ligands.

In Figure 3, the *steric properties* derived from the affinity data are displayed for CoMFA (left) and CoMSIA (right). Areas indicated by green contours correspond to regions where steric occupancy with bulky groups will increase affinity. Areas encompassed by

yellow isopleths should be sterically avoided; otherwise, reduced affinity can be expected. As becomes immediately obvious, the CoMSIA method provides more contiguous contour diagrams,⁴⁰ which allows an easier interpretation of the correlation results mapped back onto the molecular structures. Furthermore, CoMSIA isocontour diagrams lie within regions occupied by the ligands, whereas CoMFA contours highlight those areas where the ligand would interact with a possible environment. Yet, the combined application of different methods enables one to verify the convergence of the results or to complement either conclusion.⁷⁰ An example for both cases is given by the isocontour representation close to the chloro substituent of epibatidine (**1**), a very potent ligand for the (α4)₂(β2)₃ nAChR subtype. Green contours revealed by both analyses indicate that this region is favorable for steric occupancy. Yet, whereas the CoMFA contour mainly indicates that the presence of the chloro substituent is favorable, the CoMSIA contour also includes part of the aromatic ring system. This finding can be understood in considering rather low binding affinities of com-

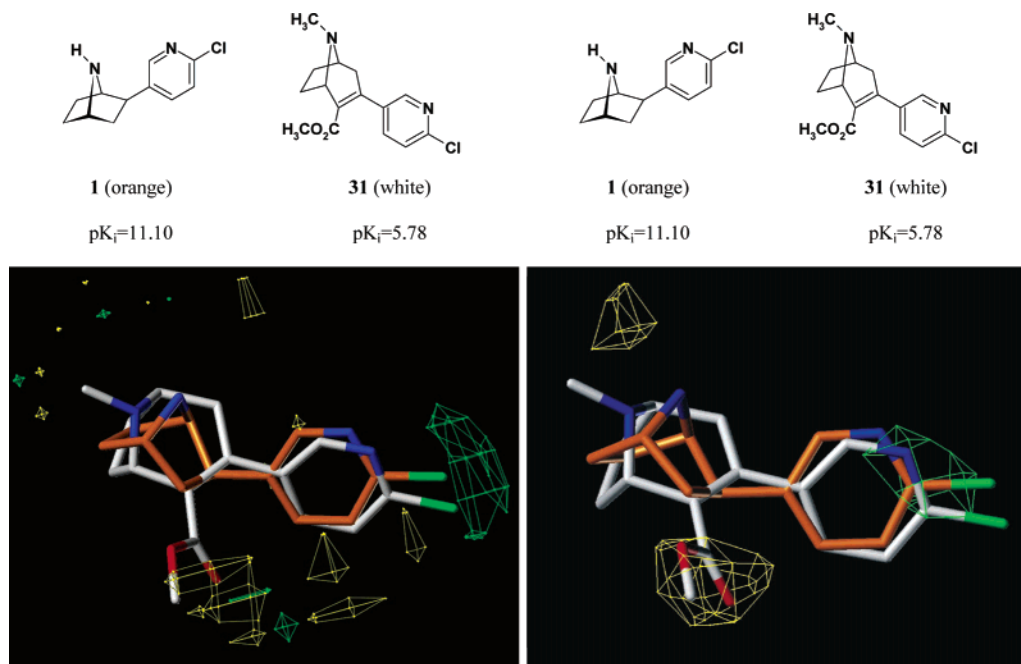


Figure 3. Stdev*coeff contour plots elucidating the steric features as obtained by CoMFA (left) and CoMSIA (right) analyses. Green isopleths (contour level: CoMFA: 0.012; CoMSIA: 0.0016⁵⁷) enclose areas where steric bulk will enhance affinity. Yellow contours (contour level: CoMFA: -0.010; CoMSIA: -0.0010) highlight areas that should be kept unoccupied, otherwise affinity will decrease. This is demonstrated by the highly affine epibatidine (**1**, orange), which orientates its chlorosubstituent toward a green area, and the weakly affine ligand **31** (white). For the latter compound, the ester moiety reaches into a yellow highlighted area.

pounds such as **17–19** or **25–28**. These compounds do not orient any molecular part into this region.

On the other hand, the less active ligand **31** orientates two substituents into or close to disfavored regions. One of these is the methyl group belonging to the nitrogen of the bicycle, which points in a direction considered to be unfavorable by the CoMSIA model. This is in agreement with findings from the CoMFA studies of Tonder et al.³³ and Glennon et al.³⁰ However, it is well known that in some cases, introduction of an *N*-methyl group increases affinity (as with (–)-nornicotine–(–)-nicotine), whereas *N*-methylation of pyrido[3,4-*b*]homotropine (PHT) or (–)-cytisine¹⁷ results in decreased affinity. Finally, in some cases *N*-methylation has little to no effect (as with (–)-epibatidine–(–)-*N*-methylepibatidine).³⁰ These findings are in agreement with a recent report that the nAChR seems quite sensitive to changes in the nature of the cationic center of the agonist.³⁵ It is important to note that, in our alignment, the very active *N*-methylepibatidine (**5**) does not orient its *N*-methyl group into the region found being sterically disallowed, whereas the less active **18**, for example, does. In that respect, considering properties of the whole ligands during superimposition, as done by RigFit, may be advantageous compared to aligning molecules solely by taking into account single pharmacophoric elements. No unequivocal answer is given by the CoMFA maps in this region. The other substituent belongs to the ester moiety. Here, both models clearly indicate that this group, being oriented in a region in front of the plane of the aromatic ring (with respect to the viewer), is disfavorable for binding.

Furthermore, CoMFA reveals two other regions that are not shown by CoMSIA. On one hand, CoMFA more distinctively elucidates that steric bulk located in the ring plane is considered favorable (as indicated by the

two smaller green contours at the bottom of the figure). These contours would thus account for the rather high affinity of **43** and **44**, for instance. On the other hand, the yellow contours to the right thereof show that steric bulk, as given by the aromatic systems of **34–37**, is less favorable in this region. This disfavorable region is also indirectly related to the 2-chloro substitution of the aromatic ring system in **12**. Steric interactions between the chlorosubstituent and the bicyclic ring system lead to a more perpendicular orientation between the aromatic moiety and the double bond in **12**, resulting in a tilt of the pyrazin ring as compared to, for example, the unsubstituted compound **9** or epibatidine (**1**). Hence, the CoMFA analysis also attributes part of the lower binding affinity of **12** to the “displaced” 5,6-region of the pyrazine moiety.

Hence, in addition to the main contours discussed first above, the steric CoMFA map reveals additional complementary information compared to the CoMSIA map. In this respect, exploiting the results of both approaches leads to a better interpretation at the 3D level of the QSAR. In any case, however, it must be remembered that all features derived from a comparative molecular field analysis are only a mirror of the structural variations inherently present in the selected data set. Accordingly, selecting another structurally deviating data set may result in different features leading to alternative conclusions.

Maps for *electrostatic properties* are shown in Figure 4. As opposed to the steric maps, CoMFA and CoMSIA reveal essentially similar results here. Hence, only a CoMSIA map is given. nAChR modulators orienting groups with increasing negative charge into areas contoured in red will enhance binding as will groups with a more positive charge placed into areas indicated in blue. A red contour extends into the area between

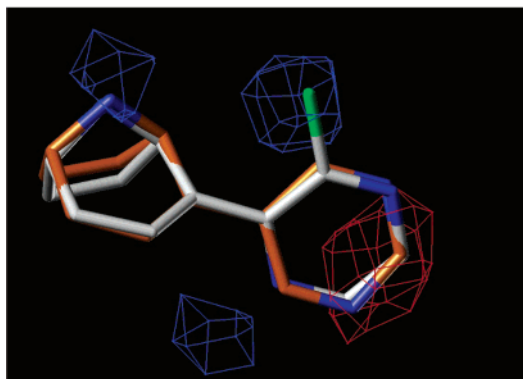
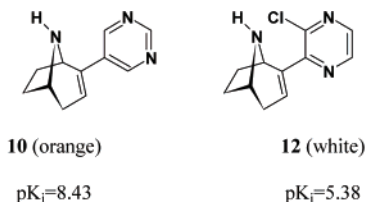


Figure 4. Contour plot of the CoMSIA stdev*coeff for the electrostatic properties. Red isopleths (contour level -0.007^{57}) encompass regions where an increase of negative charge will enhance affinity, whereas in blue-contoured areas (contour level 0.006), more positive charges are favorable for binding properties. Part of the pyrimidine substituent of **10** (orange) lies within a red area favorable for negative charge. The chlorosubstituent of the weakly affine **12** (white), on the other hand, reaches into a blue area. Similarly, the nitrogens of the bicycles are within a region that indicates that an increase in positive charge will result in higher affinity of both compounds.

both nitrogens of the pyrimidine moiety of compounds such as **10**. The result may be interpreted in light of our recent findings,¹⁸ in that in a series of diazine-containing compounds such as **22**, **23**, and **24**, the nitrogens of the pyrimidine moiety show by far the most negative atomic charge compared to the ones of the pyridazine or pyrazine substituents (also see the interpretation of the “lower” contour obtained for the hydrogen bond acceptor properties (Figure 6) (below)). Corresponding to earlier results,³³ this red area is also in the vicinity of the halogen substituent of compounds **1–7**, which, carrying high electron density, is favorable. The blue isopleths around the basic nitrogen atom of the bicycles clearly indicate that, in this region, a positive charge is mandatory for activity. On the other hand, the chlorosubstituent of the 2-chloro-3-pyrazinyl moiety of the less active ligand **12** proved to be unfavorable. Accordingly, the blue contour at the bottom of Figure 4 indicates that substituents with high electron density (such as the ester moiety of **31**) are also unfavorable in this region.

White and yellow contours in Figure 5 indicate areas where *hydrophilic* and *hydrophobic* properties are preferred, respectively. Most of the aromatic moiety of **1** and its halogen substituent are surrounded by a yellow isopleths. This large contour does not seem to be able to discriminate between molecules with an aromatic moiety attached to the bicyclic system via a pivot bond. In fact, visual inspection of all those molecules indicate that, in all cases, the aromatic moiety orients at least one carbon atom into this region. However, molecules such as **8**, **17**, or **25** do not have a lipophilic moiety in that area. Hence, the yellow contour indicates that a missing part leads to the reduced binding affinities in

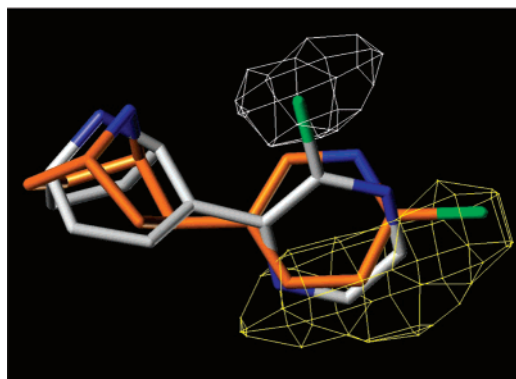
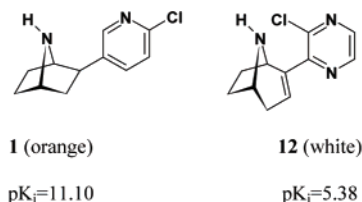


Figure 5. Contour plot of the CoMSIA stdev*coeff for the hydrophobic properties. Yellow isopleths (contour level 0.015⁵⁷) encompass regions favorable for hydrophobic groups. In white-contoured areas (contour level -0.005), more hydrophilic groups are favorable for binding properties. For the aromatic moieties, a picture similar to the electrostatic properties (see Figure 4) appears for epibatidine (**1**, orange) and **12** (white).

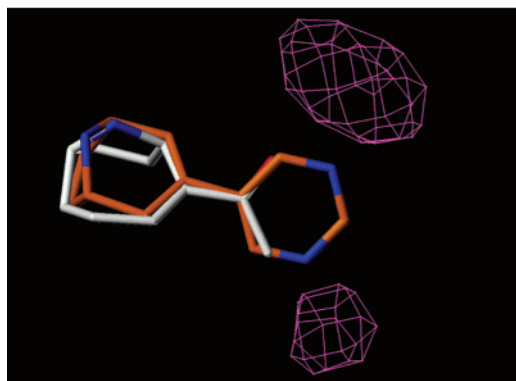
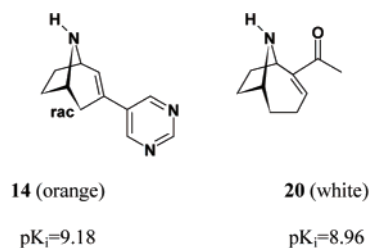


Figure 6. CoMSIA stdev*coeff contour plot for the hydrogen bond acceptor properties. Isopleths in magenta (contour level⁵⁷ 0.01) represent regions of hydrogen bond donors on the receptor site. The carbonyl oxygen of anatoxin-a (**20**, white), as well as the nitrogens of the pyrimidine-moiety of **14** (orange), both highly affine ligands for the $(\alpha 4)_2(\beta 2)_3$ nAChR subtype, are oriented toward these areas.

these cases. Finally, the chlorosubstituent of the pyrazinyl moieties in **12** and **16** as well as to some extent the sulfur in **19** is unfavorable, as indicated by the white contour.

It is interesting to compare Sheridan's model for the nicotinic pharmacophore²⁶ (see above, points A and B) with the contribution maps of the *hydrogen bonding properties*.

The contour plot for the hydrogen bond acceptor properties (Figure 6) shows two areas in magenta that represent regions of proton *donors* on the *receptor site*. Both are near the carbonyl oxygen (e.g., in anatoxin-a (**20**)) and the nitrogens of the pyrimidine moiety of **14**.¹⁹ This is in line with the fact that **14** and **20** are potent ligands of the $(\alpha 4)_2(\beta 2)_3$ nAChR subtype. The occurrence of the lower of both contours is interesting because, at a first glance, it proposes a second hydrogen bond donor site in the receptor, not yet described by current pharmacophore models.^{30,33,34} As already mentioned above, a related contour is found in the electrostatic map (Figure 4). However, an alternative and more indirect interpretation consistent with both isopleths has recently been given by us.¹⁸ The hydrogen bond acceptor capability of the heteroaromatic moiety depends on the electron density at the respective acceptor nitrogen.^{71,72} As anticipated, the mutual reduction of electron density at the ortho or para nitrogens in pyridazine or pyrazine leads to less favorable interactions with a hydrogen bond donor of the receptor side compared to the pyrimidine ring with nitrogens located in meta position.⁷² In addition, this latter explanation would also account for the *observed* high activity of pyridine-containing compounds, which lack a second nitrogen in the ring and, thus, possess a more electron-rich aromatic moiety. In that respect, it is interesting to note that at the chosen contour level, the upper isopleths comprise a larger region than the lower one, indicating the position of the upper hydrogen bond acceptor to be more important. However, underestimation of binding affinities of compounds containing nonsubstituted pyridine moieties (**46**, **51**, **53**, and **55**) and, hence, not orienting any ring nitrogen toward the lower contour may also be explained (see Design and Prediction section). In this respect, it is anticipated that including compounds with pyridine substituents into the training set will lead to a further-reduced influence attributed to the region of the lower contour.

In Figure 7, the contour plot for the hydrogen bond donor properties, the isopleths in cyan, must be regarded as regions where a proton *acceptor* on the *receptor site* can be expected. In addition, the highly affine ligands **3**¹³ and **39** are shown together with the contour diagram. The two smaller isopleths can be attributed to the basic nitrogen in the bicycle of compounds such as **3**, whereas the large isopleths result from the hydrogen bond donating group in cytosine-like compounds such as **39**. It has to be noted that the CoMSIA implementation in SYBYL takes into account a possible inversion of aliphatic amine nitrogens, which explains the occurrence of extended or multiple contours in these regions. This is also corroborated by the fact that inspection of the contour plot of the model derived from charged molecules (and, thus, having a quaternary bicycle nitrogen) (not shown) reveals a similar arrangement.

It is widely accepted (although not proven) that the binding mode of nAChR ligands encompasses a hydrogen bond between a hydrogen bond donor in the receptor and a hydrogen bond acceptor in the ligand. Numerous lines of investigations concerning interactions between nAChR modulators and their receptor published by Dougherty et al.,^{73,74} on the other hand, provide evidence

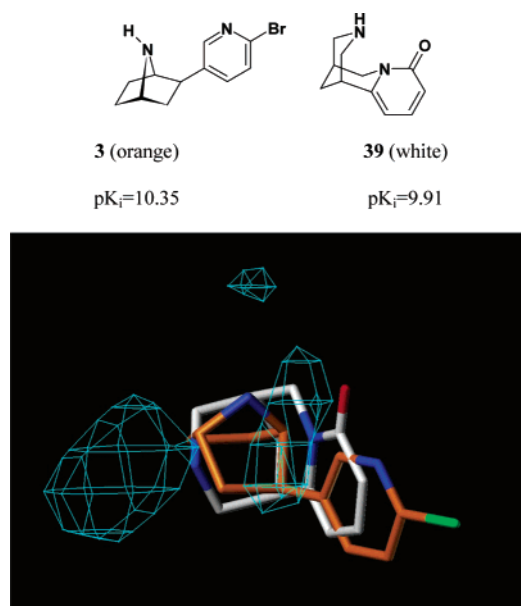


Figure 7. CoMSIA stdev*coeff contour plot for the hydrogen bond donor properties. Isopleths in cyan (contour level 0.011⁵⁷) can be regarded as areas where a proton acceptor on the receptor site is expected. According to Dougherty's investigations and the findings by Brejc et al., in these regions amino acids capable of cation- π interactions are located. The N-H bonds of the highly affine ligands **3** and **39** (taking also into account a possible inversion at the bicycle N) are pointing toward these areas.

that the cationic moieties of the nitrogen-containing bicycle of various ligands bind at the receptor through a cation- π interaction. Recently published results obtained by Brejc et al.,³¹ who succeeded in determining the three-dimensional structure of a molluscan acetylcholine-binding protein (AChBP), which is most closely related to the α -subunits of the nAChRs, corroborate this hypothesis. In that study, it was found that multiple aromatic tryptophan and tyrosine residues provide the interaction region for the positively charged quaternary ammonium group of a cocrystallized buffer molecule, which has some similarity to known receptor ligands. In that respect, it is interesting to note that the contours found in our study that describe hydrogen bond acceptor properties of the ligands are rather localized with respect to the nitrogen atoms in the aromatic rings (Figure 6), which is in agreement with the fact that hydrogen bonds are strongly directional. The isopleths for the hydrogen bond donor properties, however, appear more widespread around the basic nitrogen in the bicycles (Figure 7), which coincide with the less strongly directional character of an interaction between a cation and the negative electrostatic potential on the face of an aromatic ring.⁷⁴ In fact, while for ACh a potent cation- π interaction with α Trp143 has been identified in (muscle-type) nAChR, no such singular interaction is as yet evident for nicotine.^{35,36}

Design and Prediction. Consulting all contribution maps, especially those for steric, electrostatic, and hydrophobic properties, one region seems to be particularly interesting for substitution: the para position to the pivot bond of the aromatic moiety. Considering these findings, we introduced a chlorosubstituent in the 2-position of the pyrimidine-ring of ligands **10**,²⁰ **14**, and **23**,^{11,18} which should result in compounds **50**, **52**, and

54 with higher binding affinity. In the case of **50**, the affinity is indeed improved by 0.3 orders of magnitude (pK_i). Ligands **52** and **54**, however, only show binding affinities equal to those of **14** and **23**.

Furthermore, to investigate the importance of a substituent at the para position of the aromatic moiety, the chlorosubstituents of compounds **1** and **21**⁸ were removed, leading to the pyridine-containing ligands **46**¹³ (already known) and **55**.^{11,18} Compounds **51** and **53**,⁷⁵ the latter previously known but not tested in our radioligand binding assay, were also included in the test set because of their pyridine moiety. For all of these ligands, binding affinities were underestimated by the QSAR models, although only **55** deviates by more than one logarithmic unit in both the CoMFA and CoMSIA models. In view of the restricted training set not comprising any of these nonsubstituted pyridine derivatives, the uncertainty in the affinity prediction of these compounds is not unexpected. Recently, we have shown that subtle electrostatic effects at the heterene nitrogens influence the binding affinity of compounds of a homologous series (see above). These subtle effects may not have been incorporated in our models for nonsubstituted pyridine-containing molecules because of the missing training data.

Compounds **48** and **49** were suitable to investigate the influence of the removal of the *N*-methyl group compared to **18** and **19**. Different tendencies are shown. The desmethylated thioamide **49** is more affine than **19**. In contrast, in the case of the amides **18** and **48**, the removal of the methyl group decreases affinity. This opposing (and unexpected) trend leads to the largest deviation between experimentally determined and calculated pK_i values found for all compounds of the test set in the case of **48**.

Thus far, the composition of our test set is primarily determined by the newly designed compounds. In this respect, we were interested in obtaining highly active compounds. To obtain a more uniformly distributed pK_i range that allows a more stringent evaluation of the predictive power of our models, the test set was extended to 22 compounds. The predicted affinities of the already-known isoxazole-containing **47**¹⁶ and ligands **56–67** are also reported in Table 1. No compound of the training set contains an isoxazole moiety. Yet, the error in the predicted binding affinity amounts to less than 0.8 logarithmic units as determined for **47** by both QSAR models. Of the other compounds, only **63** in the case of CoMFA and **57** and **63** in the case of CoMSIA, respectively, show errors in the predicted pK_i values that are considerably larger than one logarithmic unit. The magnitude of these errors should be related, however, to the range of pK_i values covered by the test set ligands, which amounts to almost 7 logarithmic units. Additionally, apart from the pyridine-containing compounds discussed above, no systematic trend in the residuals across different classes of compounds can be observed.

Finally, considering all compounds of the test set together, predictive r^2 values of 0.614 and 0.660 for CoMFA and CoMSIA, respectively, are found. Hence, both models again show considerable predictive power, with better performance obtained by the CoMSIA model, as might have already been anticipated from the slightly

higher q^2 value found for the latter analysis (Table 3). Obviously, for CoMSIA, the different functional form used to evaluate molecular similarity in space, together with the more distinctive property fields, results in a more robust 3D QSAR model, compared to the one obtained with CoMFA.

Conclusions

Two new 3D QSAR models (CoMFA and CoMSIA) of convincing predictive power were developed for $(\alpha_4)_2(\beta_2)_3$ nAChR ligands. For the first time, field contribution maps for hydrophobic and hydrogen bond donor and acceptor properties were generated for nAChR ligands that allow a more detailed understanding of their binding affinities in structural terms. The hydrogen bond property fields may especially be regarded as a corroboration of current pharmacophore models. In addition, electrostatic and hydrogen bond acceptor fields in particular provide an explanation for the general trends observed in binding affinity upon modifications of the heteroaromatic moieties.

The properly selected training set of 45 structurally varying nAChR modulators included 16 ligands (**12–16**, **18**, **19**, and **29–37**) reported for the first time in this study. The same holds for 14 out of the 22 ligands in the test set (**47–52**, **54**, **56**, and **58–63**). Thus, interpreting the field contribution maps of the statistically significant QSAR models, ideas for some of these new ligands such as **48–52** and **54** were generated, and their syntheses described herein. Replacing the acetyl unit of (–)-ferruginine (**8**) with a dimethyl carboxamid or thiocarboxamid moiety, as in **18** and **19**, leads to a diminished binding potency as compared to **8**. Investigating the influence of the removal of the *N*-8-methyl group, the affinity decreased in the case of **48** (compared to **18**) and increased in the case of **49** (compared to **19**). Using the vinyl triflates **71**, **79**, and **84** as versatile building blocks, the novel chlorodiazine-containing nAChR ligands **12**, **16**, **50**, **52**, and **54** were easily accessible. The Pd-catalyzed Stille or Suzuki cross-couplings constitute the key reactions.

Unfortunately, only one of the designed nAChR ligands, the ferrugininoid **50**, showed a significant improvement of affinity, whereas the affinities of ligands with structural elements not represented in the training set were underestimated. However, with increasing structural and energetic data available, the current 3D QSAR models based on a still-limited training set will be improved in the future.

Experimental Section

For general procedures, in vitro binding studies, membrane preparation, binding assays, and data analysis, see ref 18.

(1*R*)-8-Methyl-8-azabicyclo[3.2.1]oct-2-ene-2-carboxylic Acid Dimethylamide (18). A suspension of anhydroegonin·HCl (**68**) (609 mg, 3 mmol) and dimethylammoniumchloride (489 mg, 6 mmol) in dry benzene (10 mL) was heated to 50 °C under an atmosphere of argon. Thionyl chloride (0.42 mL, 5.4 mmol) was added dropwise. The mixture was stirred at reflux for 3 h. The volatile components were removed in vacuo, and the residue was purified by column chromatography on silica gel (column, 3 cm × 15 cm; eluant, CH₂Cl₂/CH₃OH/concentrated aqueous NH₃ = 95:5:1) to yield a brown oil (408 mg, 69%). R_f = 0.36 (eluant CH₂Cl₂/CH₃OH/concentrated aqueous NH₃ = 95:5:1). $[\alpha]_D^{20}$ = –73.8° (*c* 0.1, CH₂Cl₂). IR (film): ν (cm^{–1}) = 2942, 1610, 1500. ¹H NMR (500 MHz,

CDCl₃): δ 1.59–1.63 (m, 1H), 1.79 (dd, $^3J = 4.0$ Hz, $^2J = 18.7$ Hz, 1H), 2.10–2.21 (m, 3H), 2.44 (s, 3H), 2.65 (m, 1H), 2.91 (m, 3H), 3.04 (m, 3H), 3.32–3.33 (m, 1H), 3.52 (d, $^3J = 4.6$ Hz, 1H), 5.71 (t, $^3J = 2.9$ Hz, 1H). ¹³C NMR (125.8 MHz, CDCl₃): δ 29.5, 30.7, 34.2, 34.9, 36.1, 38.9, 57.6, 60.7, 124.4, 136.4, 170.2. MS (70 eV), m/z (%): 194 (94, M⁺), 150 (100). HRMS calcd for C₁₁H₁₈N₂O: 194.1419. Found: 194.1417.

(1R)-2-Dimethylcarbamoyl-8-azabicyclo[3.2.1]oct-2-ene-8-carboxylic Acid Ethyl Ester (69). To a stirred solution of the amide **18** (800 mg, 4.1 mmol) in dry benzene (10 mL) were added ethyl chloroformate (0.8 mL, 8.2 mmol) and K₂CO₃ (140 mg, 1 mmol). The mixture was heated at reflux under argon for 12 h, cooled to room temperature, and filtered. The filtrate was washed with 2.0 M aqueous hydrochloric acid (30 mL), and the aqueous wash was re-extracted with benzene (30 mL). The combined organic layers were washed with saturated aqueous NaHCO₃ (30 mL) and with brine (20 mL), then dried with MgSO₄, filtered, and evaporated. The residue was purified by flash chromatography on silica gel (column, 3 cm × 15 cm; eluant, ethyl acetate) to yield a slightly brown oil (570 mg, 55%). $R_f = 0.27$ (eluant, ethyl acetate). $[\alpha]^{20}_D -49.0^\circ$ (*c* 0.49, CH₂Cl₂). IR (film): ν (cm⁻¹) = 2981, 2955, 2836, 1738, 1695, 1650, 1618. ¹H NMR (400 MHz, CDCl₃): δ 1.19–1.22 (m, 3H), 1.67–1.69 (m, 1H), 1.87 (dd, $^3J = 5.6$ Hz, $^2J = 22.8$ Hz, 1H), 2.05–2.17, 2.24–2.31 (2m, 3H), 2.69–2.85 (m, 1H), 2.95–3.02 (m, 6H), 4.07–4.13 (m, 2H), 4.31–4.38 (m, 1H), 4.43 (d, $^3J = 5.6$ Hz, 1H), 5.63 (bs, 1H). ¹³C NMR (100.5 MHz, CDCl₃, 2 rotamers): **a**: δ 14.1, 29.4, 33.2, 33.6, 35.2, 38.5, 52.0, 54.7, 60.3, 124.1, 140.0, 154.2, 170.0; **b**: δ = 14.6, 30.2, 33.3, 34.8, 35.9, 38.8, 52.0, 54.7, 61.0, 125.2, 141.2, 154.3, 170.0. MS (70 eV), m/z (%): 252 (34, M⁺), 208 (100). HRMS (M⁺) calcd for C₁₃H₂₀N₂O₃: 252.1474. Found: 252.1485.

(1R)-8-Azabicyclo[3.2.1]oct-2-ene-carboxylic Acid Dimethylamide (48). Following the procedure described for the preparation of **12**, 172 mg (95%) of **48** was obtained as a slightly yellow oil from 260 mg (1 mmol) of **69**. $R_f = 0.37$ (eluant, CH₂Cl₂/CH₃OH/concentrated aqueous NH₃ = 92.5:7.5:1). $[\alpha]^{20}_D -106.2^\circ$ (*c* 0.28, CH₂Cl₂). IR (film): ν (cm⁻¹) = 3020, 2943, 2828, 1650, 1611. UV (CH₂Cl₂): λ_{max} (log ϵ) = 277 (3.08). ¹H NMR (500 MHz, CDCl₃): δ 1.55–1.60 (m, 1H), 1.84–1.92, 1.97–2.04, 2.10–2.15 (3m, 4H), 2.50–2.54 (m, 1H), 2.93–2.99 (m, 6H), 3.65–3.67 (m, 1H), 3.75 (d, $^3J = 6.0$ Hz, 1H), 5.57–5.58 (m, 1H), NH signal not visible. ¹³C NMR (100.5 MHz, CDCl₃): δ 30.3, 35.1, 35.3, 36.0, 39.1, 52.4, 55.0, 124.3, 141.5, 170.7. MS (70 eV), m/z (%): 180 (58, M⁺), 136 (100). HRMS calcd for C₁₀H₁₆N₂O: 180.1263. Found: 180.1303.

(1R)-8-Methyl-8-azabicyclo[3.2.1]oct-2-ene-2-thiocarboxylic Acid Dimethylamide (19). A mixture of P₄S₁₀ (470 mg, 1.1 mmol) and NaF (86 mg, 2 mmol) in dry DME (8 mL) was stirred at room temperature until a clear solution was obtained (about 1.5 h). A solution of the amide **18** (150 mg, 0.72 mmol) in dry DME (5 mL) was added, and stirring was continued for 20 h. A solution of saturated aqueous Na₂CO₃ (15 mL) was added, and the resulting mixture was extracted with diethyl ether (2 × 20 mL) and CH₂Cl₂ (20 mL). The organic layer was dried with Na₂SO₄, filtered, and concentrated in vacuo. Column chromatographic purification on silica gel (column, 2 cm × 15 cm; eluant, CH₂Cl₂/CH₃OH/concentrated aqueous NH₃ = 95:5:1) yielded a yellow oil (46 mg, 32%). $R_f = 0.6$ (eluant, CH₂Cl₂/CH₃OH/concentrated aqueous NH₃ = 95:5:1). $[\alpha]^{20}_D -67.4^\circ$ (*c* 0.35, CH₂Cl₂). IR (film): ν (cm⁻¹) = 2933, 2795, 1631, 1516. UV (CH₂Cl₂): λ_{max} (log ϵ) = 285 nm (4.03). ¹H NMR (500 MHz, CDCl₃): δ 1.59–1.63 (m, 1H), 1.73 (dd, $^3J = 4.9$ Hz, $^2J = 23.7$ Hz, 1H), 2.10–2.26 (m, 3H), 2.44 (s, 3H), 2.46 (m, 1H), 3.23–3.26 (m, 1H), 3.36 (s, 3H), 3.44 (s, 3H), 3.57 (d, $^3J = 6.9$ Hz, 1H), 5.47 (s, 1H). ¹³C NMR (125.8 MHz, CDCl₃): δ 29.9, 30.0, 34.6, 35.9, 42.6, 43.1, 56.8, 62.5, 119.6, 143.4, 201.0. MS (70 eV), m/z (%): 210 (100, M⁺). HRMS calcd for C₁₁H₁₈N₂S: 210.1191. Found: 210.1203.

(1R)-8-Azabicyclo[3.2.1]oct-2-ene-2-thiocarboxylic Acid Dimethylamide (49). Following the procedure described for the preparation of thioamide **19**, 105 mg (73%) of the title compound **49** was obtained as a slightly yellow oil from 132 mg (0.73 mmol) of the amide **48**. $R_f = 0.38$ (eluant, CH₂Cl₂/

CH₃OH/concentrated aqueous NH₃ = 90:10:1). $[\alpha]^{20}_D -60.6^\circ$ (*c* 0.24, CH₂Cl₂). IR (film): ν (cm⁻¹) = 2960, 2928, 1700, 1685. UV (CH₂Cl₂): λ_{max} (log ϵ) = 286 nm (3.79). ¹H NMR (500 MHz, CDCl₃): δ 1.65–1.71 (m, 1H), 1.94–2.13, 2.38–2.47 (2m, 4H), 2.61–2.65 (m, 1H), 3.33 (s, 3H), 3.41 (s, 3H), 3.81 (t, $^3J = 6.0$ Hz, 1H), 3.93 (d, $^3J = 6.0$ Hz, 1H), 5.43 (d, $^3J = 3.4$ Hz, 1H), NH signal not visible. ¹³C NMR (125.8 MHz, CDCl₃): δ 29.7, 34.5, 35.7, 42.7, 43.4, 52.2, 56.7, 120.0, 146.3, 199.3. MS (70 eV), m/z (%): 196 (100, M⁺). HRMS calcd for C₁₀H₁₆N₂S: 196.1034. Found: 196.1042.

2-Tributylstannyl-3-chloropyrazine (72). A solution of *n*-BuLi in hexanes (2.4 M, 1.5 mL, 4.8 mmol) was added to cool (–10 °C) dry THF (30 mL) under an atmosphere of argon. The mixture was cooled to –70 °C, and TMP (0.44 mL, 2.6 mmol) was added. After the mixture was warmed to 0 °C, the solution was stirred for 30 min and then cooled to –70 °C again. 2-Chloropyrazine (230 μ L, 2 mmol) in dry THF (3 mL) and tributyltinchloride (0.52 mL, 2.4 mmol) were added, and stirring was continued for 2.5 h at –70 °C and for 12 h at room temperature. The mixture was cooled to –60 °C, a mixture of THF (5 mL) and water (1 mL) was added, the solution was slowly warmed to room temperature, and the volatile components were removed in vacuo. The residue was dissolved in CH₂Cl₂ (30 mL), and the resulting solution was washed with water (2 × 20 mL). The organic layer was dried with MgSO₄ (5 g), the suspension was filtered, volatile components of the filtrate were removed in vacuo, and the residue was purified by column chromatography (column, 2 cm × 15 cm; eluant, (1) *n*-hexane, (2) *n*-hexane/ethyl acetate = 1:1). A yellow oil was obtained (330 mg, 40%). $R_f = 0.18$ (eluant, *n*-hexane). ¹H NMR (400 MHz, CDCl₃): δ = 0.85 (t, $^3J = 7.3$ Hz, 9H), 1.19–1.23 (m, 6H), 1.25–1.34 (m, 6H), 1.51–1.58 (m, 6H), 8.13, 8.58 (2d, $^3J = 2.4$ Hz, 2H). ¹³C NMR (100.5 MHz, CDCl₃): δ = 10.8 (3C), 13.6 (3C), 27.2 (3C), 29.0 (3C), 141.7, 143.9, 157.6, 172.1. MS (70 eV), m/z (%): 403 (1, M⁺), 269 (100). HRMS calcd for C₁₆H₂₉ClIn₂Sn: 401.0957. Found: 401.0944.

The following general procedures were used to prepare all compounds shown in Scheme 2 and are illustrated by the conversion of vinyl triflate **71** via **73** to the ligand **12** as a specific example. Characterization data for individual compounds are then listed below.

General Procedure 1. Pd(0)-mediated cross-coupling of the vinyl triflates **71**,²⁰ **79**,¹⁹ and **84**^{16,18} to the tributylstannylchlorodiazines **72** and **74** to give the carbamates **73**, **75**, **80**, **81**, and **85**.

(1R)-2-(3'-Chloropyrazin-2'-yl)-8-azabicyclo[3.2.1]oct-2-ene-8-carboxylic Acid Ethyl Ester (73). A solution of bis(benzonitrile)palladium(II) chloride (25 mg, 0.08 mmol), CuI (18 mg, 0.15 mmol), Ph₃As (42 mg, 0.13 mmol), LiCl (120 mg, 2.9 mmol), and triflate **71** (330 mg, 1.0 mmol) in anhydrous degassed DMF (1 mL) under argon was immersed in an oil bath and maintained at a temperature of 80 °C. A solution of the organostannane **72** (460 mg, 1.14 mmol) was added dropwise. After the mixture was stirred for 14 h at 85 °C, the black slurry was allowed to cool to room temperature. A solution of KF (200 mg) in dry CH₃OH (10 mL) was added, and the mixture was stirred for 40 min. Ethyl acetate was added (25 mL), the mixture was filtered, the volatile components were removed in vacuo, and the residue was purified by flash chromatography on silica gel (column, 2 cm × 18 cm; eluant, *n*-hexane/ethyl acetate = 4:1) to yield a colorless oil (177 mg, 60%). $R_f = 0.23$ (eluant, *n*-hexane/ethyl acetate = 4:1). $[\alpha]^{20}_D -80.3^\circ$ (*c* 0.2, CH₂Cl₂). IR (film): ν (cm⁻¹) = 2979, 1699, 1385. UV (CH₂Cl₂): λ_{max} (log ϵ) = 281 nm (3.57). ¹H NMR (400 MHz, CDCl₃): δ 1.21–1.34 (m, 3H), 1.58–1.77 (m, 2H), 2.01–2.22 (m, 3H), 2.91–3.02 (m, 1H), 4.09–4.14 (m, 2H), 4.43–4.48 (m, 1H), 4.89–5.01 (m, 1H), 6.39–6.40 (m, 1H), 8.19 (bs, 1H), 8.45 (d, $^3J = 2.5$ Hz, 1H). ¹³C NMR (125.8 MHz, CDCl₃): δ 14.7, 27.8, 29.7, 35.6, 52.0, 55.4, 61.0, 130.0, 141.2, 141.7, 142.3, 144.5, 146.8, 148.2. MS (70 eV), m/z (%): 293 (100, M⁺). HRMS calcd for C₁₄H₁₆ClN₃O₂: 293.0931. Found: 293.0924.

(1R)-2-(2'-Chloropyrimidin-5'-yl)-8-azabicyclo[3.2.1]oct-2-en-8-carboxylic Acid Ethyl Ester (75): colorless oil,

isolated in 54% yield from 320 mg (0.96 mmol) of vinyl triflate **71**. $R_f = 0.38$ (eluant, *n*-hexane/ethyl acetate = 2:1). $[\alpha]_D^{20} = -141.8^\circ$ (*c* 0.15, CH₂Cl₂). IR (film): ν (cm⁻¹) = 3034, 2982, 2913, 2833, 1700, 1634. UV (CH₂Cl₂): λ_{max} (log ϵ) = 251 nm (4.06). ¹H NMR (400 MHz, CDCl₃): δ 1.21–1.25 (t, ³*J* = 7.2 Hz, 3H), 1.75–1.78 (m, 1H), 1.91–2.06 (m, 2H), 2.15–2.30 (m, 2H), 2.71–3.05 (m, 1H), 4.06–4.15 (m, 2H), 4.41–4.44 (m, 1H), 4.69–4.74 (m, 1H), 5.90–5.91 (m, 1H), 8.58 (s, 2H). ¹³C NMR (100.5 MHz, CDCl₃): δ 14.7, 29.8, 34.0, 34.8, 51.9, 55.0, 60.3, 61.3, 125.5, 131.0, 137.6, 154.6, 156.0, 160.0. MS (70 eV), *m/z* (%): 293 (100, M⁺). HRMS calcd for C₁₄H₁₆ClN₃O₂: 293.0931. Found: 293.0928.

(±)-3-(3'-Chloropyrazin-2'-yl)-8-azabicyclo[3.2.1]oct-2-ene-8-carboxylic Acid Ethyl Ester (**80**): slightly yellow oil, isolated in 83% yield from 330 mg (1.0 mmol) of vinyl triflate **79**. $R_f = 0.41$ (eluant, *n*-hexane/ethyl acetate = 2:1). IR (film): ν (cm⁻¹) = 3046, 2978, 1699, 1515. UV (CH₂Cl₂): λ_{max} (log ϵ) = 284 nm (3.88). ¹H NMR (500 MHz, CDCl₃): δ 1.24 (t, ³*J* = 7.1 Hz, 3H), 1.80–1.85 (m, 1H), 2.01–2.07 (m, 2H), 2.20–2.33 (m, 2H), 3.04–3.12 (m, 1H), 4.13 (q, ³*J* = 7.1 Hz, 2H), 4.48–4.63 (m, 2H), 6.58–6.66 (m, 1H), 8.20, 8.42 (2d, ³*J* = 2.4 Hz, 2H). ¹³C NMR (125.8 MHz, CDCl₃): δ 14.7, 29.3, 34.7, 35.7, 52.1, 53.0, 61.1, 131.9, 136.3, 141.6, 141.7, 147.1, 153.1, 154.4. MS (70 eV), *m/z* (%): 293 (62, M⁺), 192 (100). HRMS calcd for C₁₄H₁₆N₃O₂Cl: 293.0931. Found: 293.0941.

(±)-3-(2'-Chloropyrimidin-5'-yl)-8-azabicyclo[3.2.1]oct-2-ene-8-carboxylic Acid Ethyl Ester (**81**): colorless oil, isolated in 73% yield from 330 mg (1 mmol) of vinyl triflate **79**. $R_f = 0.3$ (eluant: *n*-hexane/ethyl acetate = 2:1). IR (film): ν (cm⁻¹) = 3037, 2980, 2957, 2872, 1736, 1694. UV (CH₂Cl₂): λ_{max} (log ϵ) = 265 nm (4.04). ¹H NMR (400 MHz, CDCl₃): δ 1.22 (t, ³*J* = 7.2 Hz, 3H), 1.68–1.74 (m, 1H), 1.94–2.06 (m, 2H), 2.13–2.26 (m, 2H), 3.07 (bs, 1H), 4.11 (q, ³*J* = 7.1 Hz, 2H), 4.58 (bs, 2H), 6.56 (s, 1H), 8.54 (s, 2H). ¹³C NMR (100.5 MHz, CDCl₃): δ 14.6, 29.6, 34.5, 35.2, 51.6, 53.0, 61.2, 127.3, 131.5, 132.6, 154.2, 155.6 (2C), 159.9. MS (70 eV), *m/z* (%): 293 (9, M⁺), 84 (100). HRMS calcd for C₁₄H₁₆ClN₃O₂: 293.0931. Found: 293.0922.

(1*R*)-2-(2'-Chloropyrimidin-5'-yl)-9-azabicyclo[4.2.1]non-2-ene-9-carboxylic Acid Ethyl Ester (**85**). The reaction was carried out for 12 h at 80 °C. The resulting carbamate was crystallized from *n*-hexane/ethyl acetate for several times. Colorless powder, isolated in 64% yield from 315 mg (0.92 mmol) of vinyl triflate **84**. $R_f = 0.42$ (eluant, *n*-hexane/ethyl acetate = 2:1). Mp 127–129 °C. $[\alpha]_D^{20} = -55.5^\circ$ (*c* 0.24, CH₂Cl₂). IR (KBr): ν (cm⁻¹) = 2982, 2918, 1686, 1570. ¹H NMR (400 MHz, CDCl₃, 2 rotamers, ratio 1:1): δ 1.15–1.19 and 1.22–1.25 (2 m, 3H), 1.62–2.46 (m, 8H), 4.07–4.15 (m, 2H), 4.44–4.47 and 4.53–4.55 (2m, 1H), 4.70 and 4.75 (2d, ³*J* = 9.2 Hz, 1H), 5.88–5.94 (m, 1H), 8.63 and 8.78 (2s, 2H). ¹³C NMR (100.5 MHz, CDCl₃, 2 rotamers, ratio 1:1): **a**: δ 13.5, 24.3, 28.1, 30.3, 31.3, 56.3, 57.8, 61.1, 131.8, 134.3, 142.4, 153.2, 156.8 (2C), 159.6; **b**: δ 14.8, 24.4, 29.1, 31.1, 32.2, 56.6, 58.4, 61.2, 132.4, 134.3, 143.2, 153.9, 157.5 (2C), 159.6. MS (70 eV), *m/z* (%): 307 (47, M⁺), 41 (100). HRMS calcd for C₁₅H₁₈ClN₃O₂: 307.1088. Found: 307.1071.

(1*R*)-2-(3'-Pyridinyl)-8-azabicyclo[3.2.1]oct-2-en-8-carboxylic Acid Ethyl Ester (**77**). To a solution of triflate **71** (330 mg, 1 mmol) in dry THF (5 mL) were successively added bis(triphenylphosphane)palladium(II) chloride (8 mg, 0.01 mmol), 3-diethylboranylpyridine (**76**, 220 mg, 1.5 mmol), and 2 M aqueous Na₂CO₃ solution (2 mL, 4 mmol). The mixture was heated at 85 °C for 20 min. Diethyl ether (10 mL) and water (5 mL) were added and the phases separated. The organic layer was dried with Na₂SO₄, the suspension was filtered, and the filtrate was concentrated in vacuo. The crude product was purified by column chromatography on silica gel (column, 3 cm × 15 cm; eluant, (1) *n*-hexane/ethyl acetate = 1:1, (2) ethyl acetate) to yield a colorless oil (196 mg, 76%). $R_f = 0.54$ (eluant, ethyl acetate). $[\alpha]_D^{20} = -143.2^\circ$ (*c* 0.17, CH₂Cl₂). IR (film): ν (cm⁻¹) = 2982, 2835, 1700, 1588. ¹H NMR (500 MHz, CDCl₃): δ 1.18–1.29 (m, 3H), 1.68–1.79 (m, 1H), 1.93–2.02 (m, 2H), 2.07–2.18 (m, 1H), 2.21–2.31 (m, 1H), 2.79–3.01 (m, 1H), 4.09 (q, ³*J* = 6.7 Hz, 2H), 4.33–4.48 (m,

1H), 4.69–4.85 (m, 1H), 5.76 (t, ³*J* = 3.3 Hz, 1H), 7.19–7.21 (m, 1H), 7.58–7.74 (m, 1H), 8.43 (s, 1H), 8.54 (d, ⁴*J* = 1.9 Hz, 1H). ¹³C NMR (125.8 MHz, CDCl₃): δ 14.1, 29.7, 33.9, 34.7, 52.1, 55.4, 61.1, 121.7, 123.3, 132.0, 134.6, 141.2, 146.9, 148.5, 154.6. MS (70 eV), *m/z* (%): 258 (100, M⁺). HRMS calcd for C₁₅H₁₈N₂O₂: 258.1368. Found: 258.1362.

3-(3'-Pyridinyl)-8-azabicyclo[3.2.1]oct-2-ene-8-carboxylic Acid Ethyl Ester (**82**). Following the procedure described for the preparation of carbamate **77**, 195 mg (75%) of **82** was obtained as a slightly yellow oil from 330 mg (1 mmol) of vinyl triflate **79**. $R_f = 0.57$ (eluant, ethyl acetate). IR (film): ν (cm⁻¹) = 2979, 2913, 2872, 1707, 1631. UV (CH₂Cl₂): λ_{max} (log ϵ) = 251 nm (4.05). ¹H NMR (500 MHz, CDCl₃): δ 1.22 (t, ³*J* = 7.1 Hz, 3H), 1.66–1.76 (m, 1H), 1.93–2.04 (m, 2H), 2.20–2.28 (m, 2H), 2.97–3.20 (m, 1H), 4.12 (q, ³*J* = 7.1 Hz, 2H), 4.49–4.65 (m, 2H), 6.43–6.52 (m, 1H), 7.19 (dd, ³*J* = 4.7 Hz, ³*J* = 8.0 Hz, 1H), 7.58 (d, ³*J* = 8.0 Hz, 1H), 8.44 (dd, ²*J* = 1.4 Hz, ³*J* = 4.7 Hz, 1H), 8.57 (s, 1H). ¹³C NMR (125.8 MHz, CDCl₃): δ 14.6, 29.3, 34.1, 35.5, 51.8, 53.1, 61.0, 123.1, 129.7, 130.2, 132.0, 135.1, 146.5, 148.5, 154.3. MS (70 eV), *m/z* (%): 258 (60, M⁺), 229 (100). HRMS calcd for C₁₅H₁₈N₂O₂: 258.1368. Found: 258.1360.

(1*R*)-2-(3'-Chloropyrazin-2'-yl)-8-azabicyclo[3.2.1]oct-2-ene (**12**). In a sealed vessel, carbamate **73** (80 mg, 0.27 mmol) and concentrated hydrochloric acid (37%, 5 mL, saturated with argon) were heated at 80 °C for 1 h. The volatile components were removed in vacuo. Water was added, and the aqueous solution was washed with CH₂Cl₂ (5 mL). Then concentrated aqueous NH₃ was added to the aqueous layer until a pH of ~9 was reached. The aqueous layer was extracted with CH₂Cl₂ (3 × 5 mL), the organic phase was dried with Na₂SO₄, the suspension was filtered, the solvent was evaporated, and the residue was purified by column chromatography on silica gel (column, 1 cm × 15 cm; eluant, CH₂Cl₂/CH₃OH/concentrated aqueous NH₃ = 95:5:1) to yield the free base as colorless crystals (37 mg, 59%). $R_f = 0.62$ (eluant, CH₂Cl₂/CH₃OH/concentrated aqueous NH₃ = 90:10:1). Mp 97 °C. $[\alpha]_D^{20} = -22.0^\circ$ (*c* = 0.1 CH₂Cl₂). IR (KBr): ν (cm⁻¹) = 2925, 1730, 1381. UV (CH₂Cl₂): λ_{max} (log ϵ) = 287 nm (3.27). ¹H NMR (500 MHz): δ 1.66–1.69 (m, 1H), 2.02–2.09 (m, 4H), 2.50–2.70 (m, 1H), 2.71–2.75 (d, ²*J* = 21.2 Hz, 1H), 3.78–3.80 (t, ³*J* = 6.0 Hz, 1H), 4.19–4.20 (d, ³*J* = 6.0 Hz, 1H), 6.23–6.24 (m, 1H), 8.16 (d, ³*J* = 2.4 Hz, 1H), 8.40 (d, ³*J* = 2.4 Hz, 1H). ¹³C NMR (125.8 MHz, CDCl₃): δ 30.2, 35.5, 35.7, 52.5, 55.8, 128.8, 141.3, 141.6, 141.7, 147.1, 152.3. MS (70 eV), *m/z* (%): 221 (97, M⁺), 192 (100). HRMS calcd for C₁₁H₁₂ClN₃: 221.0720. Found: 221.0718.

General Procedure 2. The TMSI-mediated cleavage of the carbamate protecting group was performed to give compounds **16** and **50–54**.

(±)-3-(3'-Chloropyrazin-2'-yl)-8-azabicyclo[3.2.1]oct-2-ene (**16**). To a solution of carbamate **80** (243 mg, 0.83 mmol) in dry, degassed CHCl₃ (5 mL) was added TMSI (240 μL, 1.7 mmol), and the resulting light brown solution was heated under argon in a sealed vessel at 85 °C for 3 h. After the mixture was cooled to ambient temperature and after evaporation of the volatile components in vacuo, a solution of HCl in diethyl ether (2 M, 0.25 mL, 0.5 mmol) in dry CH₃OH (3 mL) was added, and the resulting yellow-brown solution was stirred for 10 min at room temperature. The volatile components were removed in vacuo. After the residue was treated with water (3 mL) and the mixture was extracted with CH₂Cl₂ (3 × 5 mL), concentrated aqueous NH₃ was added to the aqueous layer until a pH of ~9 was reached, and the resulting solution was extracted with CH₂Cl₂ (5 × 2 mL). The organic layer was dried with MgSO₄, filtered, and concentrated in vacuo. The crude product was purified by column chromatography on silica gel (column, 2 cm × 15 cm; eluant, CH₂Cl₂/CH₃OH/concentrated aqueous NH₃ = 95:5:0.1).

As indicated by the spectral data, the product consisted of a mixture of two colorless solids in a ca. 9:1 ratio. The main component was separated by a second chromatographic purification on silica gel (column 1 cm × 15 cm; eluant as before) to provide compound **16** as colorless crystals (51 mg, 28%).

$R_f = 0.29$ (eluant, $\text{CH}_2\text{Cl}_2/\text{CH}_3\text{OH}/\text{concentrated aqueous NH}_3 = 95:5:0.1$). Mp 52 °C. IR (KBr): ν (cm^{-1}) = 2943, 1453, 1106. UV (CH_3OH): λ_{max} ($\log \epsilon$) = 283 nm (3.71). $^1\text{H NMR}$ (500 MHz, CDCl_3): δ 1.68–1.75 (m, 1H), 1.85–1.95 (m, 1H), 1.98–2.12 (m, 2H), 2.20–2.28 (d, $^2J = 17.6$ Hz, 1H), 2.80–2.84 (dd, $^3J = 4.2$ Hz, $^2J = 17.6$ Hz, 1H), 3.78–3.80 (m, 2H), 6.59–6.60 (m, 1H), 8.15 (d, $^3J = 2.4$ Hz, 1H), 8.37 (d, $^3J = 2.4$ Hz, 1H), NH signal not visible. $^{13}\text{C NMR}$ (125.8 MHz, CDCl_3): δ 29.9, 35.1, 37.6, 52.7, 53.4, 130.5, 139.0, 141.3, 141.7, 147.2, 153.6. MS (70 eV), m/z (%): 221 (27, M^+), 192 (100). HRMS calcd for $\text{C}_{11}\text{H}_{12}\text{ClN}_3$: 221.0720. Found: 221.0723.

For the impurity, identified as (\pm)-3-(3'-iodopyrazin-2'-yl)-8-azabicyclo[3.2.1]oct-2-ene, the following spectral data could be obtained: $^{13}\text{C NMR}$ (100.5 MHz, D_3COD): δ 29.4, 34.9, 35.0, 53.5, 56.3, 129.6, 138.8, 142.5, 142.6, 147.3, 151.1. MS (70 eV), m/z (%): 313 (2.2, M^+). HRMS calcd for $\text{C}_{11}\text{H}_{12}\text{IN}_3$: 313.0075. Found: 313.0069.

(1R)-2-(2'-Chloropyrimidin-5'-yl)-8-azabicyclo[3.2.1]oct-2-ene Hydrochloride (50): yellow, slightly hygroscopic powder, isolated in 42% yield from 118 mg (0.4 mmol) of carbamate **75**. $R_f = 0.26$ (eluant, $\text{CH}_2\text{Cl}_2/\text{CH}_3\text{OH}/\text{concentrated aqueous NH}_3 = 95:5:1$). Mp 235 °C. $[\alpha]_{\text{D}}^{20} = -72.2^\circ$ (c 0.07, H_2O). IR (KBr): ν (cm^{-1}) = 2930, 1643, 1586. UV (H_2O): λ_{max} ($\log \epsilon$) = 250 nm (4.23). $^1\text{H NMR}$ (500 MHz, D_2O): δ 2.11–2.18 (m, 1H), 2.41–2.55 (m, 3H), 2.58–2.63 (m, 1H), 3.10 (d, $^2J = 19.5$ Hz, 1H), 4.45 (d, $^3J = 5.5$ Hz, 1H), 4.85 (d, $^3J = 5.5$ Hz, 1H), 6.46 (s, 1H), 8.88 (s, 2H), NH signal not visible. $^{13}\text{C NMR}$ (125.8 MHz, D_3COD): δ 29.4, 34.3, 34.9, 55.0, 56.6, 126.6, 131.2, 133.7, 158.2 (2 C), 161.7. MS (70 eV), m/z (%): 221 (16, M^+), 36 (100). HRMS calcd for $\text{C}_{11}\text{H}_{12}\text{ClN}_3$ (free base): 221.0720. Found: 221.0708.

(1R)-2-(3'-Pyridinyl)-8-azabicyclo[3.2.1]oct-2-ene (51): colorless oil, isolated in 44% yield from 224 mg (0.87 mmol) of carbamate **77**. $R_f = 0.33$ (eluant, $\text{CH}_2\text{Cl}_2/\text{CH}_3\text{OH}/\text{concentrated aqueous NH}_3 = 95:5:1$). $[\alpha]_{\text{D}}^{20} = -74.4^\circ$ (c 0.22, CH_2Cl_2). IR (film): ν (cm^{-1}) = 2948, 2829, 1653, 1637. UV (CH_2Cl_2): λ_{max} ($\log \epsilon$) = 249 nm (4.01). $^1\text{H NMR}$ (500 MHz, CDCl_3): δ 1.73–1.78 (m, 1H), 2.08–2.21 (m, 4H), 2.73–2.77 (d, $^2J = 18.5$ Hz, 1H), 3.83–3.86 (m, 1H), 4.13 (t, $^3J = 2.9$ Hz, 1H), 5.95 (t, $^3J = 3.2$ Hz, 1H), 7.31 (dd, $^3J = 4.8$ Hz, $^3J = 8$ Hz, 1H), 7.69–7.72 (m, 1H), 8.54 (dd, $^4J = 1.6$ Hz, $^3J = 4.8$ Hz, 1H), 8.69 (d, $^4J = 1.8$ Hz, 1H). $^{13}\text{C NMR}$ (125.8 MHz, CDCl_3): δ 30.4, 35.7, 36.2, 52.5, 55.7, 121.5, 123.1, 131.9, 135.0, 142.1, 146.5, 148.0. MS (70 eV), m/z (%): 186 (82, M^+), 157 (100). HRMS calcd for $\text{C}_{12}\text{H}_{14}\text{N}_2$: 186.1157. Found: 186.1202.

(\pm)-3-(3'-Chloropyrimidin-5'-yl)-8-azabicyclo[3.2.1]oct-2-ene Hydrochloride (52): colorless crystals, isolated in 73% yield from 156 mg (0.53 mmol) of carbamate **81**. $R_f = 0.45$ (eluant, $\text{CH}_2\text{Cl}_2/\text{CH}_3\text{OH}/\text{concentrated aqueous NH}_3 = 90:10:1$). Mp > 240 °C dec. IR (KBr): ν (cm^{-1}) = 2880, 1653, 1638. UV (H_2O): λ_{max} ($\log \epsilon$) = 250 nm (4.24). $^1\text{H NMR}$ (500 MHz, D_2O): δ 2.12–2.18 (m, 1H), 2.30–2.37 (m, 1H), 2.46–2.54 (m, 2H), 2.77–2.83 (m, 1H), 3.28–3.32 (m, 1H), 4.52–4.55 (m, 1H), 4.59–4.61 (m, 1H), 6.74 (d, $^3J = 5.8$ Hz, 1H), 8.88 (s, 2H), NH signal not visible. $^{13}\text{C NMR}$ (125.8 MHz, D_2O): δ 27.8, 32.8, 34.4, 54.1, 54.5, 127.3, 128.4, 131.3, 156.0, 157.2 (2 C). MS (70 eV), m/z (%): 221 (16, M^+), 192 (100). HRMS calcd for $\text{C}_{11}\text{H}_{12}\text{ClN}_3$ (free base): 221.0720. Found: 221.0718.

(\pm)-3-(3'-Pyridinyl)-8-azabicyclo[3.2.1]oct-2-ene Maleate (53). The obtained base of **53** (94 mg, 71%) was dissolved in butanone (2 mL), and a solution of maleic acid (58 mg, 0.5 mmol) in dry butanone (2 mL) was added at 80 °C. A white precipitate formed immediately (128 mg, 59%). $R_f = 0.39$ (eluant, $\text{CH}_2\text{Cl}_2/\text{CH}_3\text{OH}/\text{concentrated aqueous NH}_3 = 90:10:1$). Mp 110–112 °C. IR (KBr): ν (cm^{-1}) = 2951, 1641, 1569. UV (CH_3OH): λ_{max} ($\log \epsilon$) = 240 nm (4.17). $^1\text{H NMR}$ (500 MHz, D_3COD): δ 1.77–1.83 (m, 1H), 1.89–2.02 (m, 1H), 2.09–2.19 (m, 2H), 2.50 (d, $^2J = 18.1$ Hz, 1H), 2.94 (dd, $^3J = 3.8$ Hz, $^2J = 18.2$ Hz, 1H), 4.13 (t, $^3J = 6.1$ Hz, 1H), 4.19 (t, $^3J = 5.8$ Hz, 1H), 6.26 (s, 2H), 6.33–6.34 (m, 1H), 7.24–7.26 (m, 1H), 7.74–7.77 (m, 1H), 8.27–8.28 (m, 1H), 8.44 (d, $^4J = 2.3$ Hz, 1H). $^{13}\text{C NMR}$ (125.8 MHz, D_3COD): δ 28.9, 34.0, 34.9, 55.1, 55.5, 125.5, 126.2, 133.1 (2 C), 135.4, 136.1 (2C), 146.9, 149.6,

170.6 (2C). MS (70 eV), m/z (%): 186 (16, M^+), 157 (100). HRMS calcd for $\text{C}_{12}\text{H}_{14}\text{N}_2$ (free base): 186.1157. Found: 186.1180.

(1R)-2-(2'-Chloropyrimidin-5'-yl)-9-azabicyclo[4.2.1]non-2-ene Hydrochloride (54). Carbamate **85** (70 mg, 0.23 mmol) was dissolved in dry, degassed CHCl_3 (5 mL). After addition of TMSI (67 μL , 0.44 mmol), the resulting light brown solution was heated under argon in a sealed vessel at 80 °C for 3 h. After the mixture was cooled to ambient temperature, the volatile components were removed in vacuo (1.5 h). Aqueous hydrochloric acid (1 M, 0.5 mL, 0.5 mmol) was added, and the mixture was again concentrated in vacuo (1.5 h) to yield a colorless oil (35 mg, 64%). $R_f = 0.33$ (eluant, $\text{CH}_2\text{Cl}_2/\text{CH}_3\text{OH}/\text{concentrated aqueous NH}_3 = 95:5:1$). $[\alpha]_{\text{D}}^{20} = 24.6^\circ$ (c 0.21, CH_3OH). IR (film): ν (cm^{-1}) = 3423, 2925, 1635. UV (CH_2Cl_2): λ_{max} ($\log \epsilon$) = 252 nm (3.81). $^1\text{H NMR}$ (500 MHz, CDCl_3): δ 1.92–1.95, 2.14–2.18, 2.29–2.31, 2.54–2.65 (4m, 8H), 4.35–4.36 (m, 1H), 4.68–4.70 (m, 1H), 6.44–6.46 (m, 1H), 8.70, 8.79, 9.03 (3s, 2H). $^{13}\text{C NMR}$ (125.8 MHz, CDCl_3): δ 23.7, 27.8, 28.4, 31.0, 58.6, 58.7, 133.8, 136.7, 136.9, 157.2 (2 C), 160.2. MS (70 eV), m/z (%): 236 (24, M^+), 202 (100). HRMS calcd for $\text{C}_{12}\text{H}_{14}\text{ClN}_3$ (free base): 235.0876. Found: 235.0864.

Acknowledgment. We thank the Deutsche Forschungsgemeinschaft and the Fonds der Chemischen Industrie for generous financial support, the Boehringer Ingelheim Pharma KG for generous gifts of tropinone, the Bayer AG, Solvay GmbH, Merck AG, and Degussa AG for gifts of various chemicals. S.S. thanks the DPhG-Stiftung im Stifterverband für die Deutsche Wissenschaft for fellowship support.

Supporting Information Available: ^1H and ^{13}C NMR spectra of compounds **12**, **16**, **18**, **19**, and **48–54**. Two tables with statistical data for “leave-five-out” cross-validation runs as well as CoMFA and CoMSIA analyses with doubled K_i values for compounds **1–7**, **13–16**, and **26**. This material is available free of charge via the Internet at <http://pubs.acs.org>.

References

- Holladay, M. W.; Dart, M. J.; Lynch, J. K. Neuronal Nicotinic Acetylcholine Receptors as Targets for Drug Discovery. *J. Med. Chem.* **1997**, *40*, 4169–4194.
- Lin, N.-H.; Meyer, M. D. Recent Developments in Neuronal Nicotinic Acetylcholine Receptor Modulators. *Exp. Opin. Ther. Patents* **1998**, *8*, 991–1015.
- Schmitt, J. D. Exploring the Nature of Molecular Recognition in Nicotinic Acetylcholine Receptors. *Curr. Med. Chem.* **2000**, *7*, 749–800.
- Tønder, J. E.; Olesen, P. H. Agonists at the $\alpha 4\beta 2$ Nicotinic Acetylcholine Receptors: Structure-Activity Relationships and Molecular Modelling. *Curr. Med. Chem.* **2001**, *8*, 651–674.
- Spande, T. F.; Garaffo, H. M.; Edward, M. W.; Yeh, H. J. C.; Pannell, L.; Daly, J. W. Epibatidine: A Novel (Chloropyridyl)-azabicycloheptane with Potent Analgesic Activity from an Ecuadorian Poison Frog. *J. Am. Chem. Soc.* **1992**, *114*, 3475–3478.
- Decker, M. W.; Meyer, M. D. Therapeutic Potential of Neuronal Nicotinic Acetylcholine Receptor Agonists as Novel Analgesics. *Biochem. Pharmacol.* **1999**, *58*, 917–923.
- Bannon, A. W.; Decker, M. W.; Holladay, M. W.; Curzon, P.; Donnelly-Roberts, D.; Puttfarcken, P. S.; Bitner, R. S.; Diaz, A.; Dickenson, A. H.; Porsolt, R. D.; Williams, M.; Arneric, S. P. Broad-Spectrum, Nonopioid Analgesic Activity by Selective Modulation of Neuronal Nicotinic Acetylcholine Receptors. *Science* **1998**, *279*, 77–81.
- Wright, E.; Gallagher, T.; Sharples, C. G. V.; Wonnacott, S. Synthesis of UB-165: A Novel Nicotinic Ligand and Anatoxina-Epipatidine Hybrid. *Bioorg. Med. Chem. Lett.* **1997**, *7*, 2867–2870.
- Meyer, D. M.; Decker, M. W.; Rueter, L. E.; Anderson, D. J.; Dart, M. J.; Kim, K. H.; Sullivan, J. P.; Williams, M. The Identification of Novel Structural Compound Classes Exhibiting High Affinity for Neuronal Nicotinic Acetylcholine Receptors and Analgesic Efficacy in Preclinical Models of Pain. *Eur. J. Pharmacol.* **2000**, *393*, 171–177.

- (10) Liang, F.; Navarro, H. A.; Abraham, P.; Kotian, P.; Ding, Y.-S.; Fowler, J.; Volkow, N.; Kuhar, M. J.; Carroll, F. I. Synthesis and Nicotinic Acetylcholine Receptor Binding Properties of *exo*-2-(2'-Fluoro-5'-pyridinyl)-7-azabicyclo[2.2.1]heptane: A New Positron Emission Tomography Ligand for Nicotinic Receptors. *J. Med. Chem.* **1997**, *40*, 2293–2295.
- (11) Sharpless, C. G. V.; Karig, G.; Simpson, G. L.; Spencer, J. A.; Wright, E.; Milar, N. S.; Wonnacott, S.; Gallagher, T. Synthesis and Pharmacological Characterization of Novel Analogues of the Nicotinic Acetylcholine Receptor Agonist (\pm)-UB-165. *J. Med. Chem.* **2002**, *45*, 3235–3245.
- (12) Koskinen, A. M. P.; Rapoport, H. Synthetic and Conformational Studies on Anatoxin-a: A Potent Acetylcholine Agonist. *J. Med. Chem.* **1985**, *28*, 1301–1309.
- (13) Horti, A. G.; Scheffel, U.; Kimes, A. S.; Musachio, J. L.; Ravert, H. T.; Mathews, W. B.; Zhan, Y.; Finley, P. A.; London, E. D.; Dannals, R. F. Synthesis and Evaluation of *N*-[¹¹C]Methylated Analogues of Epibatidine as Tracers for Positron Emission Tomographic Studies of Nicotinic Acetylcholine Receptors. *J. Med. Chem.* **1998**, *41*, 4199–4206.
- (14) Badio, B.; Garaffo, H. M.; Plummer, C. V.; Padgett, W. L.; Daly, J. W. Synthesis and Nicotinic Activity of Epiboxidine: An Isoxazole Analogue of Epibatidine. *Eur. J. Pharmacol.* **1997**, *321*, 189–194.
- (15) Che, D.; Wegge, T.; Stubbs, M. T.; Seitz, G.; Meier, H.; Methfessel, C. *exo*-2-(Pyridazin-4-yl)-7-azabicyclo[2.2.1]heptanes: Syntheses and Nicotinic Acetylcholine Receptor Agonist Activity of Potent Pyridazine Analogues of (\pm)-Epibatidine. *J. Med. Chem.* **2001**, *44*, 47–57.
- (16) Wegge, T. Ph.D. Thesis, Philipps-University of Marburg, 2001.
- (17) Imming, P.; Klaperski, P.; Stubbs, M. T.; Seitz, G.; Gündisch, D. Syntheses and Evaluation of Halogenated Cytisine Derivatives and of Bioisosteric Thiocytisine as Potent and Selective nAChR Ligands. *Eur. J. Med. Chem.* **2001**, *36*, 375–388.
- (18) Gohlke, H.; Gündisch, D.; Schwarz, S.; Tilotta, M. C.; Seitz, G.; Wegge, T. Synthesis and Nicotinic Binding Studies on Enantiopure Diazine Analogues of the Novel (2-Chloro-5-pyridyl)-9-azabicyclo[4.2.1]non-2-ene UB-165. *J. Med. Chem.* **2002**, *45*, 1064–1072 and references therein.
- (19) Schwarz, S. Ph.D. Thesis, Philipps-University of Marburg, 2002.
- (20) Gündisch, D.; Harms, K.; Schwarz, S.; Seitz, G.; Stubbs, M. T.; Wegge, T. Synthesis and Evaluation of Diazine Containing Bioisosteres of (–)-Ferruginine as Ligands for Nicotinic Acetylcholine Receptors. *Bioorg. Med. Chem.* **2001**, *9*, 2683–2691.
- (21) Gündisch, D.; Kämpchen, T.; Schwarz, S.; Seitz, G.; Siegl, J.; Wegge, T. Syntheses and Evaluation of Pyridazine and Pyrimidine Containing Bioisosteres of (\pm)-Pyrido[3.4-b]homotropane and Pyrido[3.4-b]tropene as Novel nAChR Ligands. *Bioorg. Med. Chem.* **2002**, *10*, 1–9.
- (22) Stehl, A. Ph.D. Thesis, Philipps-University of Marburg, 2002.
- (23) Seifert, S.; Seitz, G.; Gündisch, D.; Tilotta, M. C. Unpublished results.
- (24) Eichler, G.; Seitz, G.; Gündisch, D.; Tilotta, M. C. Unpublished results.
- (25) Seifert, S.; Gündisch, D.; Tilotta, M. C.; Seitz, G. An Improved Synthesis and In Vitro Evaluation of Quinuclidin-2-ene Based Ligands for the Nicotinic Acetylcholine Receptor. *Pharmazie* **2003**, *58*, in press.
- (26) Sheridan, R. P.; Nilakantan, R.; Dixon, J. S.; Venkataraghavan, R. The Ensemble Approach to Distance Geometry: Application to the Nicotinic Pharmacophore. *J. Med. Chem.* **1986**, *29*, 899–906.
- (27) Barlow, R. B.; Johnson, O. Relations Between Structure and Nicotine-Like Activity: X-ray Crystal Structure Analysis of (–)-Cytisine and (–)-Lobeline Hydrochloride and a Comparison with (–)-Nicotine and other Nicotine-Like Compounds. *J. Pharmacol.* **1989**, *98*, 799–808.
- (28) Dukat, M.; Damaj, M. I.; Glassco, W.; Dumas, D.; May, E. L.; Martin, B. R.; Glennon, R. A. Epibatidine: A Very High Affinity Nicotine-Receptor Ligand. *Med. Chem. Res.* **1993**, *4*, 131–139.
- (29) Glennon, R. A.; Dukat, M. Nicotine Receptor Ligands. *Med. Chem. Res.* **1996**, 465–486.
- (30) Glennon, R. A.; Herndon, J. L.; Dukat, M. Epibatidine-Aided Studies Toward Definition of a Nicotine Receptor Pharmacophore. *Med. Chem. Res.* **1994**, *4*, 461–473.
- (31) Brejč, K.; van Dijk, W. J.; Klaassen, R. V.; Schuurmans, M.; van der Oost, J.; Smit, A. B.; Sixma, T. K. Crystal Structure of an ACh-Binding Protein Reveals the Ligand-Binding Domain of Nicotinic Receptors. *Nature* **2001**, *411*, 269–276.
- (32) Le Novère, N.; Grutter, T.; Changeux, J.-P. Models of the Extracellular Domain of the Nicotinic Receptors and of Agonist- and Ca²⁺-Binding Sites. *Proc. Natl. Acad. Sci. U.S.A.* **2002**, *99*, 3210–3215.
- (33) Tønder, J. E.; Olesen, P. H.; Hansen, J. B.; Begtrup, M.; Pettersson, I. An Improved Nicotinic Pharmacophore and a Stereoselective CoMFA-Model for Nicotinic Agonists acting at the Central Nicotinic Acetylcholine Receptors Labeled by [³H]-*N*-Methyl-carbamylcholine. *J. Comput.-Aided Mol. Des.* **2001**, *15*, 247–258.
- (34) Nicolotti, O.; Pellegrini-Callace, M.; Altomare, C.; Carotti, A.; Carrieri, A.; Sanz, F. Ligands of Neuronal Nicotinic Acetylcholine Receptor (nAChR): Inferences from the Hansch and 3-D Quantitative Structure–Activity Relationship (QSAR) Models. *Curr. Med. Chem.* **2002**, *9*, 1–29.
- (35) Beene, D. L.; Brandt, G. S.; Zhong, W.; Zacharias, N. M.; Lester, H. A.; Dougherty, D. A. Cation– π Interactions in Ligand Recognition by Serotonergic (5-HT_{3A}) and Nicotinic Acetylcholine Receptors: The Anomalous Binding Properties of Nicotine. *Biochemistry* **2002**, *41*, 10262–10269.
- (36) Pettersson, E. J.; Choi, A.; Dahan, D. S.; Lester, H. A.; Dougherty, D. A. A Perturbed pK_a at the Binding Site of the Nicotinic Acetylcholine Receptor: Implications for Nicotine Binding. *J. Am. Chem. Soc.* **2002**, *124*, 12662–12663.
- (37) Cramer, R. D., III; Patterson, D. E.; Bunce, J. D. Comparative Molecular Field Analysis (CoMFA). 1. Effect of Shape on Binding of Steroids to Carrier Proteins. *J. Am. Chem. Soc.* **1988**, *110*, 5959–5967.
- (38) Klebe, G.; Abraham, U.; Mietzner, T. Molecular Similarity Indices in a Comparative Analysis (CoMSIA) of Drug Molecules to Correlate and Predict Their Biological Activity. *J. Med. Chem.* **1994**, *37*, 4130–4146.
- (39) Klebe, G.; Abraham, U. Comparative Molecular Similarity Indices Analysis (CoMSIA) To Study Hydrogen-Bonding Properties and To Score Combinatorial Libraries. *J. Comput.-Aided Mol. Des.* **1999**, *13*, 1–10.
- (40) Böhm, M.; Stürzebecher, J.; Klebe, G. Three-Dimensional Quantitative Structure–Activity Relationship Analyses Using Comparative Molecular Field Analysis and Comparative Molecular Similarity Indices Analysis to Elucidate Selectivity Differences of Inhibitors Binding to Trypsin, Thrombin, and Factor Xa. *J. Med. Chem.* **1999**, *42*, 458–477.
- (41) SYBYL Molecular Modeling Software, version 6.6; Tripos Inc.: St. Louis, MO, 2000.
- (42) Kim, K. H.; Greco, G.; Novellino, A. Critical Review of Recent CoMFA Applications. In *3D QSAR in Drug Design*; Kubinyi, H., Folkers, G., Martin, Y. C., Eds.; Kluwer Academic Publishers: Dordrecht, The Netherlands, 1998; Vol. 3.
- (43) Bick, I. R. C.; Gillard, J. W.; Leow, H.-M. Alkaloids of *Darlingia darlingiana*. *Aust. J. Chem.* **1979**, *32*, 2523–2536.
- (44) Wegge, T.; Schwarz, S.; Seitz, G. A New and Efficient Synthetic Route to Enantiopure (+)-Anatoxin-a from (–)-Cocaine Hydrochloride. *Tetrahedron: Asymmetry* **2000**, *11*, 1405–1410 and references therein.
- (45) Stewart, J. J. MOPAC: A General Molecular Orbital Package, version 6.0; QCPE #445; J. Frank Seiler Research Laboratory, U.S. Air Force Academy, CO.
- (46) Stewart, J. J. MOPAC: A Semiempirical Molecular Orbital Program. *J. Comput.-Aided Mol. Des.* **1990**, *4*, 1–105.
- (47) Dewar, M. J. S.; Zoebisch, E. G.; Healy, E. F.; Stewart, J. J. P. AM1: A New General Purpose Quantum Mechanical Molecular Model. *J. Am. Chem. Soc.* **1985**, *107*, 3902–3909.
- (48) Lemmen, C.; Hiller, C.; Lengauer, T. RigiFit: A New Approach to Superimposing Ligand Molecules. *J. Comput.-Aided Mol. Des.* **1998**, *12*, 491–502.
- (49) Klebe, G.; Mietzner, T.; Weber, F. Methodological Developments and Strategies for a Fast Flexible Superposition of Drug-Size Molecules. *J. Comput.-Aided Mol. Des.* **1999**, *13*, 35–49.
- (50) Kearsley, S. K.; Smith, G. M. An Alternative Method for the Alignment of Molecular Structures: Maximizing Electrostatic and Steric Overlap. *Tetrahedron Comput. Methodol.* **1990**, *3*, 615–633.
- (51) Oprea, T. I.; Waller, C. L. Theoretical and Practical Aspects of Three-Dimensional Quantitative Structure–Activity Relationships. In *Reviews in Computational Chemistry*; Lipkowitz, K. B., Toyd, D. B., Eds.; Wiley-VCH: New York, 1997; Vol. 11.
- (52) Thibaut, U.; Folkers, G.; Klebe, G.; Kubinyi, H.; Merz, A.; Rognan, D. Recommendations to CoMFA Studies and 3D QSAR Publications. In *3D QSAR in Drug Design. Theory, Methods and Applications*; Kubinyi, H., Ed.; ESCOM: Leiden, The Netherlands, 1993; pp 711–716.
- (53) Wold, S.; Ruhe, A.; Wold, H.; Dunn, W. J., III. The Collinearity Problem in Linear Regression. The Partial Least Squares Approach to Generalized Inverses. *SIAM J. Sci. Statist. Comput.* **1984**, *5*, 735–743.
- (54) Stahle, L.; Wold, S. Multivariate Data Analysis and Experimental Design in Biochemical Research. *Prog. Med. Chem.* **1988**, *25*, 291–338.
- (55) Bush, B. L.; Nachbar, R. B., Jr. Sample-Distance Partial Least Squares: PLS Optimized for Many Variables, with Application to CoMFA. *J. Comput.-Aided Mol. Des.* **1993**, *7*, 587–619.

- (56) Hodgson, D. M.; Maxwell, C. R.; Wisedale, R.; Matthews, I. R.; Carpenter, K. J.; Dickenson, A. H.; Wonnacott, S. 6-Substituted 2-Azabicyclo[2.2.1]hept-5-enes by Nitrogen-Directed Radical Rearrangement: Synthesis of an Epibatidine Analogue with High Binding Affinity at the Nicotinic Acetylcholine Receptor. *J. Chem. Soc., Perkin Trans. 1* **2001**, 3150–3158.
- (57) The contour levels of CoMFA contour maps are given normally in kcal/mol. Because the CoMSIA similarity indices fields are defined in arbitrary units, they do not correspond to any potential describing different partitions of molecular interactions such as CoMFA. Consequently, the CoMSIA contour levels are given without any units.
- (58) Wenger, B. W.; Bryant, D. L.; Boyd, R. T.; McKay, D. B. Evidence for Spare Nicotinic Acetylcholine Receptors and a $\beta 4$ Subunit in Bovine Adrenal Chromaffin Cells: Studies Using Bromoacetylcholine, Epibatidine, Cytisine and mAb35. *J. Pharmacol. Exp. Ther.* **1997**, *281*, 905–913.
- (59) Houghtling, R. A.; Davila-Garcia, M. I.; Kellar, K. J. Characterization of (\pm)- ^3H]Epibatidine Binding to Nicotinic Cholinergic Receptors in Rat and Human Brain. *Mol. Pharmacol.* **1995**, *48*, 280–287.
- (60) Marks, M. J.; Smith, K. W.; Collins, A. C. Differential Agonist Inhibition Identifies Multiple Epibatidine Binding Sites in Mouse Brain. *J. Pharmacol. Exp. Ther.* **1998**, *285*, 377–386.
- (61) Sihver, W.; Gillberg, P. G.; Nordberg, A. Laminar Distribution of Nicotinic Receptor Subtypes in Human Cerebral Cortex as Determined by ^3H -($-$)-Nicotine, ^3H]Cytisine and (\pm)- ^3H]Epibatidine In Vitro Autoradiography. *Neuroscience* **1998**, *85*, 1121–1133.
- (62) Whiteaker, P.; Sharples, C. G.; Wonnacott, S. Agonist-Induced Upregulation of $\alpha 4\beta 2$ Nicotinic Acetylcholine Receptors in M10 cells: Pharmacological and Spatial Definition. *Mol. Pharmacol.* **1998**, *53*, 950–962.
- (63) Zhang, C.; Lomenzo, S. A.; Ballay, C. J., II; Trudell, M. L. An Improved Synthesis of (+)-2-Tropinone. *J. Org. Chem.* **1997**, *62*, 7888–7889.
- (64) Hartke, K.; Gerber, H. D. Tetracosphorus Decasulfide, Revival of an Old Thionating Agent. *J. Prakt. Chem./Chem.-Ztg.* **1996**, *338*, 763–765.
- (65) Bai, D.; Xu, R.; Chu, C.; Zhu, X. Synthesis of (\pm)-Epibatidine and Its Analogues. *J. Org. Chem.* **1996**, *61*, 4600–4606.
- (66) Lott, R. S.; Chauhan, V. S.; Stammer, C. H. Trimethylsilyl Iodide as a Peptide Deblocking Agent. *J. Chem. Soc., Chem. Commun.* **1979**, 495–496.
- (67) Stille, J. K. Palladium-Catalyzed Coupling Reactions of Organic Electrophiles with Organo-Stannanes. *Angew. Chem., Int. Ed. Engl.* **1986**, *25*, 508–524.
- (68) Oh-e, T.; Miyaura, N.; Suzuki, A. Palladium-Catalyzed Cross-Coupling Reaction of Organoboron Compounds with Organic Triflates. *J. Org. Chem.* **1993**, *58*, 2201–2208.
- (69) Böhm, M.; Klebe, G. Development of New Hydrogen-Bond Descriptors and Their Application to Comparative Molecular Field Analyses. *J. Med. Chem.* **2002**, *45*, 1585–1597.
- (70) Boulamwini, J. K.; Assefa, H. CoMFA and CoMSIA 3D QSAR and Docking Studies on Conformationally-Restrained Cinnamoyl HIV-1 Integrase Inhibitors: Exploration of a Binding Mode at the Active Site. *J. Med. Chem.* **2002**, *45*, 841–852.
- (71) Mecozzi, S.; West, A. P., Jr.; Dougherty, D. A. Cation- π Interactions in Aromatics of Biological and Medicinal Interest: Electrostatic Potential Surfaces as a Useful Qualitative Guide. *Proc. Natl. Acad. Sci. U.S.A.* **1996**, *93*, 10566–10571.
- (72) Nobeli, I.; Price, S. L.; Lommerse, J. P. M.; Taylor, R. Hydrogen Bonding Properties of Oxygen and Nitrogen Acceptors in Aromatic Heterocycles. *J. Comput. Chem.* **1997**, *18*, 2060–2074.
- (73) Dougherty, D. A. Cation- π Interactions in Chemistry and Biology: A New View of Benzene, Phe, Tyr, and Trp. *Science* **1996**, *271*, 163–168.
- (74) Gallivan, J. P.; Dougherty, D. A. Cation- π Interactions in Structural Biology. *Proc. Natl. Acad. Sci. U.S.A.* **1999**, *96*, 9459–9464.
- (75) Nielsen, S. F.; Østergaard Nielsen, E.; Olsen, G. M.; Liljefors, T.; Peters, D. Novel Potent Ligands for the Central Nicotinic Acetylcholine Receptor: Synthesis, Receptor Binding, and 3D QSAR Analyses. *J. Med. Chem.* **2000**, *43*, 2217–2226.
- (76) Gündisch, D.; London, E. D.; Terry, P.; Hill, G. R.; Mukhin, A. G. High Affinity Binding of ^3H]Epibatidine to Rat Brain Membranes. *NeuroReport* **1999**, *10*, 1631–1636.
- (77) Cheng, Y.-C.; Prusoff, W. H. Relationship Between the Inhibition Constant (K_i) and the Concentration of Inhibitor which Causes 50% Inhibition (IC_{50}) of an Enzymatic Reaction. *Biochem. Pharmacol.* **1973**, *22*, 3099–3108.

JM020859M